# We are IntechOpen, the world's leading publisher of Open Access books
# Built by scientists, for scientists

## 6,900
Open access books available

## 186,000
International authors and editors

## 200M
Downloads

## 154
Countries delivered to

Our authors are among the

## TOP 1%
most cited scientists

## 12.2%
Contributors from top 500 universities

CLARIVATE ANALYTICS
BOOK CITATION INDEX
INDEXED

**WEB OF SCIENCE™**

Selection of our books indexed in the Book Citation Index
in Web of Science™ Core Collection (BKCI)

## Interested in publishing with us?
## Contact book.department@intechopen.com

Numbers displayed above are based on latest data collected.
For more information visit www.intechopen.com

# Turbulent Combustion Simulation by Large Eddy Simulation and Direct Numerical Simulation

Fang Wang
*Beihang University*
*China*

## 1. Introduction

Combustion is a natural phenomenon. It happens in forest, automotive engine and gas cooker. In Computational Fluid Dynamics (CFD), the combustion phenomenon complies with a set of partial differential equations. According to the resolution scale, from big to small, the simulation methods in combustion are Reynolds Averaged Navior Stokes method (RANS), Large Eddy Simulation (LES), and Direct Numerical Simulation (DNS). Combustion model research in RANS and LES was, is and will still be a hot topic.

In this chapter, an Algebraic Sub-grid Scale turbulent Combustion Model (ASSCM) for LES is brought forward. Then this model is applied to a partly diffusion jet flame and a pre-mixed flame, after that, the database of the LES simulation results is used to test a RANS turbulent combustion model closure idea. Finally, a DNS by spectral method (Xu et al, 1996) in channel flow is carried on with consideration of buoyancy effects, and the database of the DNS simulation results is used to study RANS and LES turbulent combustion models.

## 2. Turbulent combustion models in LES

The Sub-Grid Scale (SGS) turbulent combustion model is a key point in LES study. There are two methods in modelling: one is to build the turbulent combustion model for all turbulence scale, the other is to build the models for big scale and small scale separately. Generally, there are probability density function models, laminar flame-let models, eddy break up model, and ASSCM sub-grid scale model, etc.

As for probability density function models, there are filtered density function method (FDF), probability density function method (PDF), and filtered mass density function method (FMDF), which are similar methods and all rooted in the probability function. They solve the PDF transport equation by the Lagrangian Monte Carlo scheme without using the assumed PDF functions. Also the detail chemical reaction kinetics can be applied directly without models, while the mixing term and the convection term need to be closed. The value of the filtered scaler, such as the averaged temperature, can be calculated by the integration over the composition space. When the FMDF or FDF method extended into turbulent combustion SGS model, the joint probability density function of the sub-grid-scale (SGS) scalar quantities are obtained by solution of its modelled transport equation. In the work of Colucci et al 1998 and James et al 2000, the FMDF combined with detail reaction gave good prediction in temperature

and species profiles. The SGS PDF method still use Monte Carlo method to solve the transport equation of the SGS PDF function ( Gao et al 1993).  Renfo et al 2004 used this method and Smagorinsky model to predict the [OH] time series in $H_2/N_2$ jet turbulent flame. The predicted power spectral densities and the [OH] time scale are close to the measurements.

The SGS laminar flame-let model is a quick reaction model, that means it assumes that the chemical time scales are shorter than the turbulent time scales. It uses a conservation scalar, such as the mixture fraction, to define the flow variables, such as the species concentration. Assumed PDF functions, as the double-delta function, the clipped Gaussian function and the Beta-pdf function are commonly used. The filtered mixture fraction and its variance can be calculated by transport equations. The relational expression also can be defined by experimental data. DesJardin et al 1999, using the experiential expressions, simulated the ethyne-air jet flame, the temperature prediction is higher than the experimental data in some regions. Jones 2002 applied this method in jet flame and combustion chamber in gas turbine engine, with Smagorinsky turbulent model. The averaged velocity and mixture fraction are close to the experimental data. In the simulation of the gas turbine chamber, the temperature predictions are close to the experimental data in the down stream regions. The instantaneous vortex structures showed detail flow information in the combustion chamber.

The Eddy Break Up (EBU), Eddy Dissipation Concept (EDC) and other similar concept SGS model are rooted from the same type RANS model. The turbulent time scale is rescaled by the Kolmogorov turbulent time scale, and the concentrations were calculated by the filtered values. Yaga 2002 applied this model in a swirl combustion chamber with Smagorinsky turbulent model and three steps reaction kinetics. The prediction results of the temperature and the methane concentration are in good agreement with the experimental data while the CO concentration is not very well.

An ASSCM sub-grid scale model is proposed by author and colleagues. In the filtered species equation, there are two reaction terms:

$$\frac{\partial \rho \tilde{Y}_s}{\partial t} + \frac{\partial}{\partial x_j}(\rho \tilde{u}_j \tilde{Y}_s) = \frac{\partial}{\partial x_j}(\frac{\mu}{Sc_s}\frac{\partial \tilde{Y}_s}{\partial x_j}) \\ -\tilde{w}_{L,s} - w_{S,s} - \frac{\partial g_{Sj,s}}{\partial x_j}$$ (1)

The instantaneous reaction expression for s species is in the Arrhenius form:

$$w_s = B\rho^2 Y_{fu}Y_{ox}\exp(-E/RT) = \rho^2 K Y_{fu}Y_{ox}$$ (2)

B is the pre-exponential factor, E is the activation energy and R is the universal gas constant. If the fluctuation of density can be neglected, in order to shorten the expression, the exponential term and the pre-exponential factor can be merged into one parameter K. The filtered 'big' scale reaction rate is defined as:

$$\tilde{w}_{L,s} = \rho^2 \tilde{K}\tilde{Y}_{fu}\tilde{Y}_{ox}$$ (3)

The filtered SGS reaction rate is:

$$w_{S,s} = \rho^2(\widetilde{KY_{fu}Y_{ox}} - \tilde{K}\tilde{Y}_{fu}\tilde{Y}_{ox})$$ (4)

The exact expression of the SGS reaction rate is very complex. Anyway it presents the influence from the turbulent fluctuation under the grid scale. Conceptually, comparison with the Reynolds decomposition and the correlation of the turbulent fluctuation, the expression is rewritten as:

$$w_{s,s} = \rho^2 \left[ \widetilde{K}(\widetilde{Y_{fu}\widetilde{Y}_{ox}} - \widetilde{Y}_{fu}\widetilde{Y}_{ox}) + \widetilde{Y}_{ox}(\widetilde{K\widetilde{Y}_{fu}} - \widetilde{K}\widetilde{Y}_{fu}) + \widetilde{Y}_{fu}(\widetilde{K\widetilde{Y}_{ox}} - \widetilde{K}\widetilde{Y}_{ox}) \right]$$

(5)

$\widetilde{K}$ is the integral value in the control volume. The separate subtract terms in the SGS reaction rate denote the contribution from the 'small' scale turbulence fluctuation, and they can be closed by the products of the gradient of the filtered values:

$$(\widetilde{K\widetilde{Y}_{OX}} - \widetilde{K}\widetilde{Y}_{OX}) = C_{K,Y_{ox}} L_s^2 \frac{\partial \widetilde{K}}{\partial x_j} \frac{\partial \widetilde{Y}_{ox}}{\partial x_j}$$

(6)

The $C_{K,Yox}$ is the constant, between 0.05 to 0.005 and $L_s$ is the SGS mixing length.

## 3. Jet flame simulation and premixed flame simulation using LES

The ASSCM sub-grid scale turbulent combustion model is applied to a partly diffusion jet flame and a premixed flame after a bluff body. The SGS turbulent combustion model is verified by the experimental data and the LES database is used to verified the RANS turbulent combustion model. The instantaneous turbulent and flame structures are studied too. The implicit box filter function and the Smagorinsky-Lilly's eddy viscosity turbulent model are used. The Smagorinsky constant is 0.1 in this chapter. The SGS mass flux and heat flux are in gradient models. Second order upwind scheme in space, second order central difference scheme for momentum equation, second order in temporal, and PISO algorithm are used. A random velocity component, satisfying Gaussian distribution is superposed at the inlet boundary. The grid size near inlet is 0.5mm around, and under 2mm in the simulation domain. The time step is 0.1ms. Each time step, it iterated 25 steps. As a comparison, the RANS model is applied for the jet flame too.

The methane-air jet flame, the 'Flame D', is measured by the Sandia Laboratory. The sketch map of this flame is shown in the figure 1. The central flow consists of 25% methane and 75% dry air, the inlet velocity is 29.7m/s, and the inlet temperature is 294K. The annular flow velocity is 6.8m/s and its temperature is 1880K. The surrounding flow velocity is 0.9m/s, and its temperature is 291K. The exit is located at a distance of 1m from the jet exit. The methane air reaction kinetics is taken from Westbrook as:

$$w_{fu} = 2.119 \times 10^{11} Y_{ox}^{1.3} Y_{fu}^{0.2} \exp(-2.027 \times 10^8 / RT)$$

(7)

The specific heat for all the species are using subsection polynomial expression, such as the specific heat value of methane when the temperature is between 300K to 1000K:

$$C_p = 403.58 + 9.0575T - 0.014425T^2 + 1.5805 \times 10^{-5} T^3 - 6.3431 \times 10^{-9} T^4$$

(8)

Figure 2 is the averaged temperature comparison between the RANS unified second order moment (USM) transportation turbulent combustion model prediction results and the LES ASSCM turbulent combustion model prediction results with the experimental results. In

most regions the, the prediction value of the ASSCM model are very close to the experimental data. The RANS model can give the same trend of the temperature profiles.
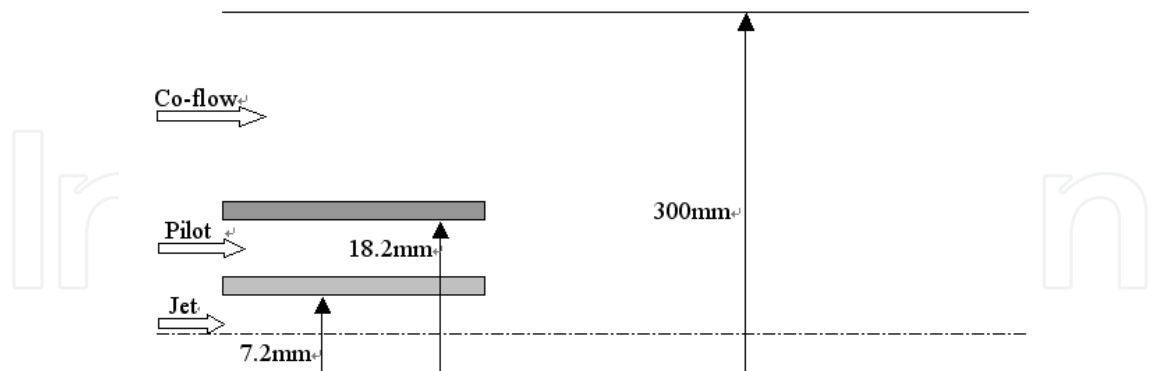


Fig. 1. The sketch map of the jet flame and its dimension.
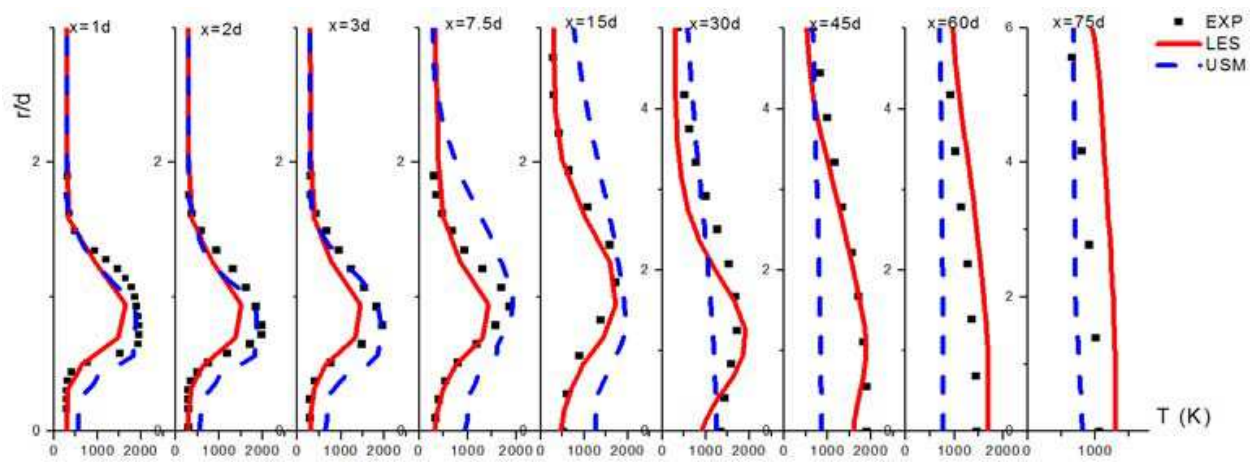


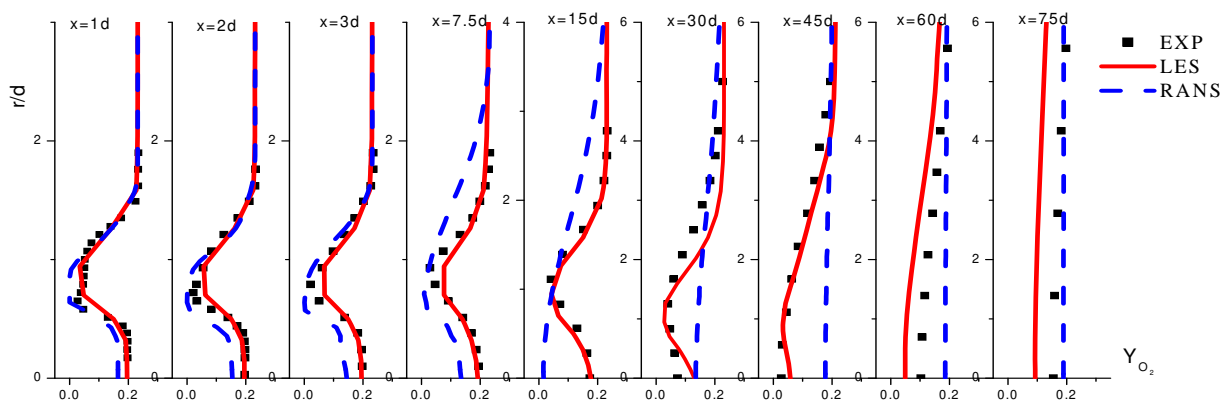Fig. 2. The average temperature profiles.



Fig. 3. The average oxygen concentration profiles.

Figure 3 shows the averaged oxygen concentration profiles comparison amongst the LES, RANS and the experimental data. In most regions, the LES ASSCM model gives good results. While the RANS predictions also are close to the experimental data in most regions. Considering RANS 1/500 computing time, it is still useful and popular in industry field. The

big difference between the RANS prediction results and the experimental data is mainly from the shear layer gradient assumption and one global step reaction kinetics.
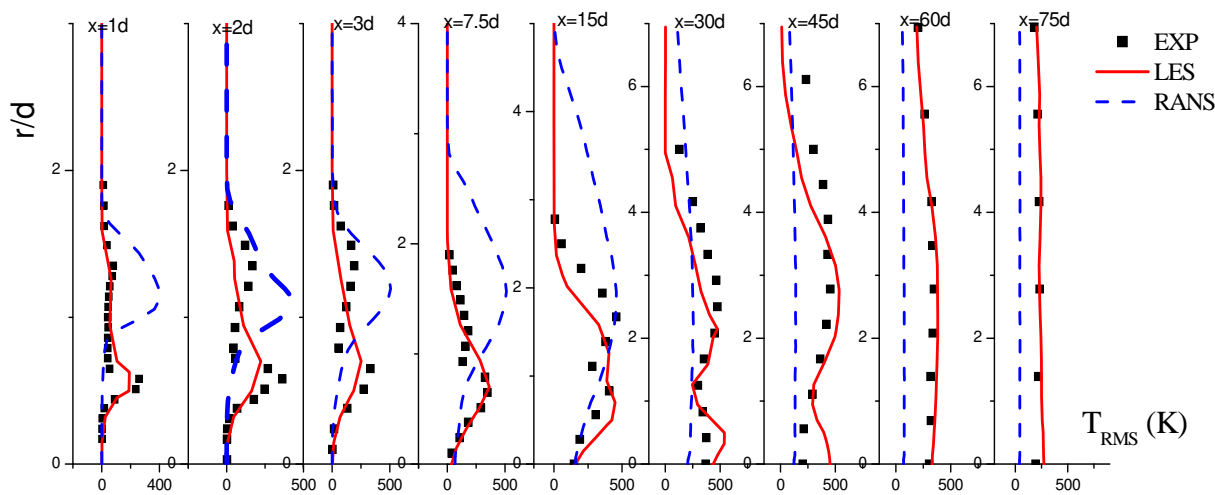


Fig. 4. The root mean square (RMS) value of the temperature.
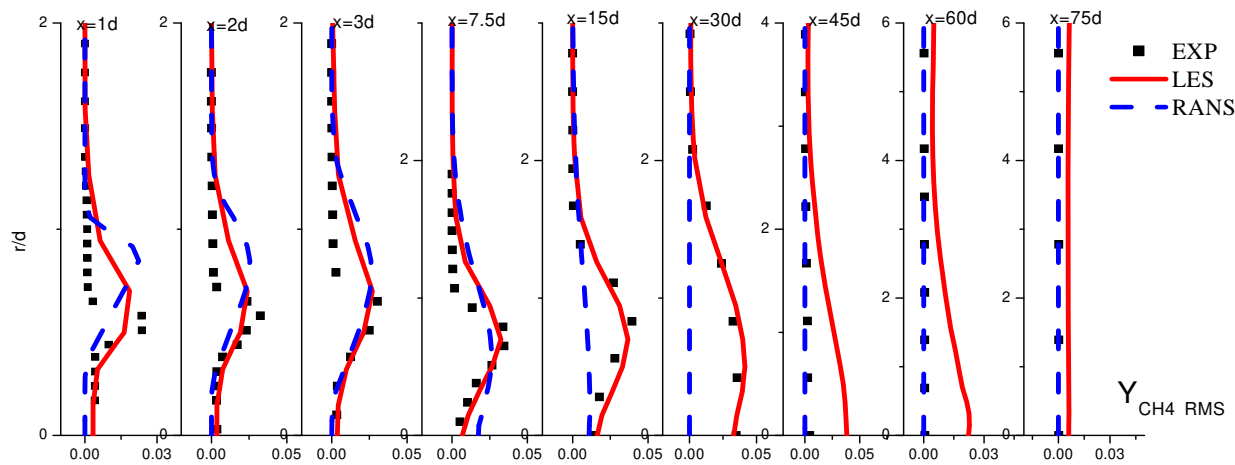


Fig. 5. The RMS value of the methane concentration.

The RMS value of the LES ASSCM model and the RANS model prediction results are shown in the figure 4 and 5, as well as the comparison with the experimental data. Generally, the LES RMS predictions are worse than the LES average value predictions, especially in the regions near the methane jet area: x=1d, x=2d, and x=3d sections. These regions have great gradient value of temperature and concentration, and there are more active turbulence fluctuations. As for the prediction of the turbulent character, the LES is much better than the RANS method.

Figure 6 is the instantaneous stain rate contour at the central axis section. The high velocity jet flow mixed with the low velocity co-flow air, then the mixing layer induced vortex and higher stain rate regions.

Figure 7 and figure 8 are instantaneous temperature contour in different time step. From these two pictures, the temperature in the central jet flow remains low for quite long distance from the inlet. The pilot flow ignite the jet flow and the flame spread downstream.
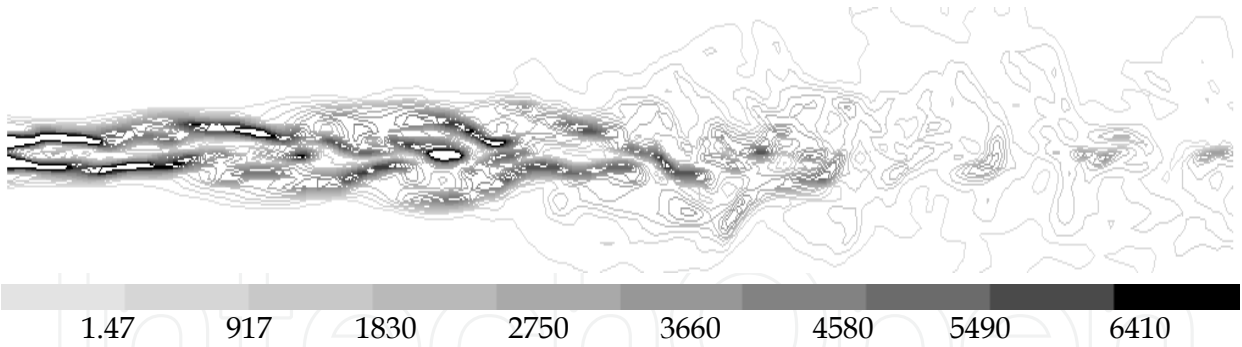
Fig. 6. The instantaneous stain rate contour (1/s).
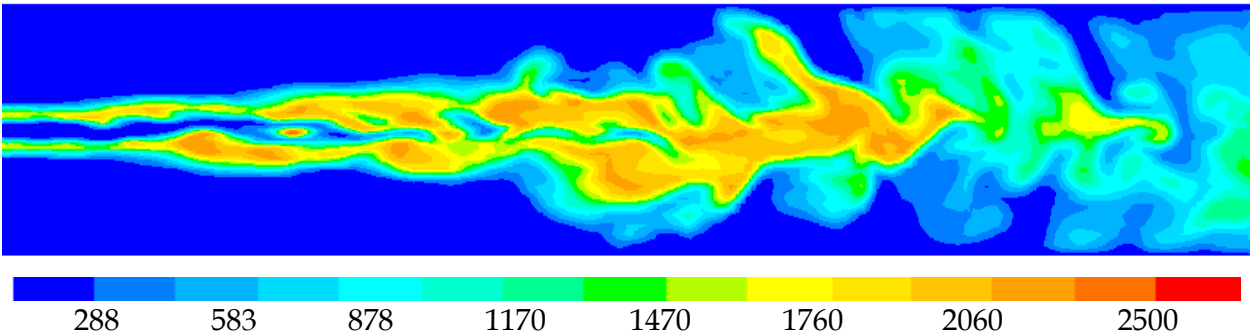


Fig. 7. The instantaneous temperature contour (K, t=0.8990s).
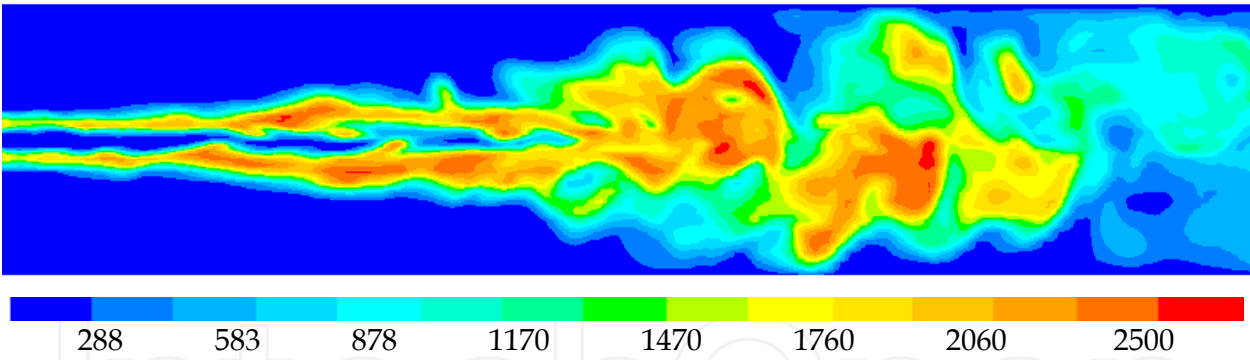


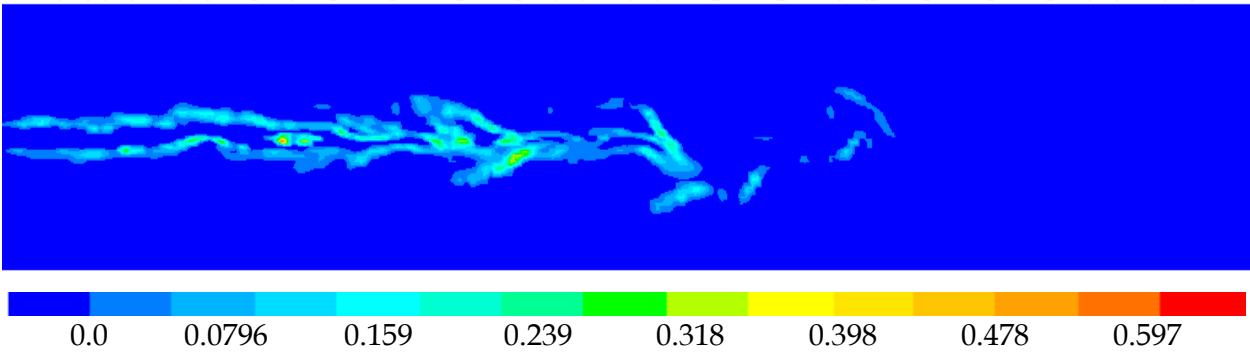Fig. 8. The instantaneous temperature contour (K, t=1.1094s).



Fig. 9. The instantaneous reaction rate contour (kmol/m³s).

The co-flow air was entraining to the combustion flames. The high temperature areas changed temporally. The unsteady flame is similar to the candle flickers. It also can be seen the wrinkle flame structures. Figure 9 is the instantaneous reaction rate contour. The high reaction rate area is the low concentration area. Reaction also happens in some isolated 'islands'.

Then, a propane air premixed flame is studied. The combustion chamber is shown in the figure 10 (Giacomazzi 2004). The inlet velocity is 17m/s, temperature is 288K, and the equivalence ratio is 0.65. The final mesh section is shown in figure 11, the maximum grid size is 0.5mm. Time step is 0.1ms, and 35 iterations during each time step.
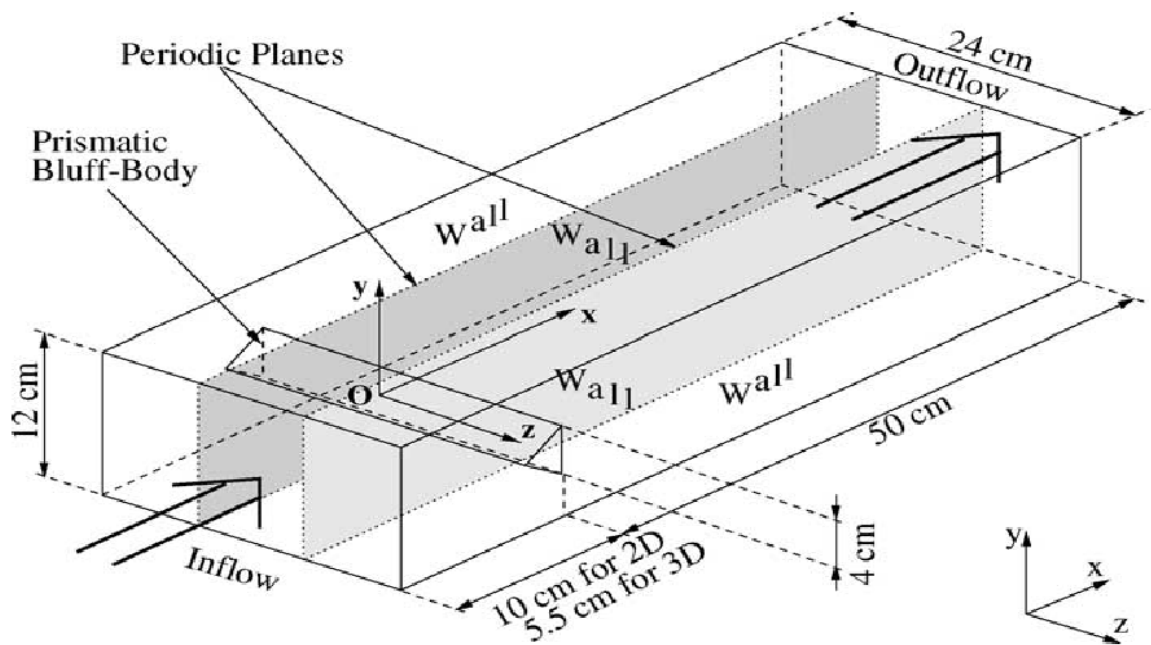


Fig. 10. The premixed chamber with bluff body (Giacomazzi 2004).
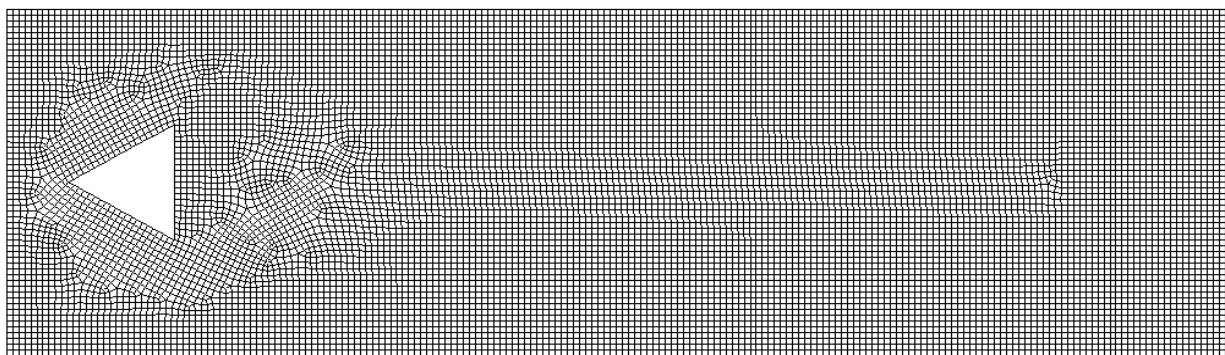


Fig. 11. The final mesh at z=0 section.

The laminar reaction rate is:

$$w_{fu} = 4.836 \times 10^9 Y_{ox}^{1.65} Y_{fu}^{0.1} \exp(-1.51 \times 10^4 / T) \tag{9}$$
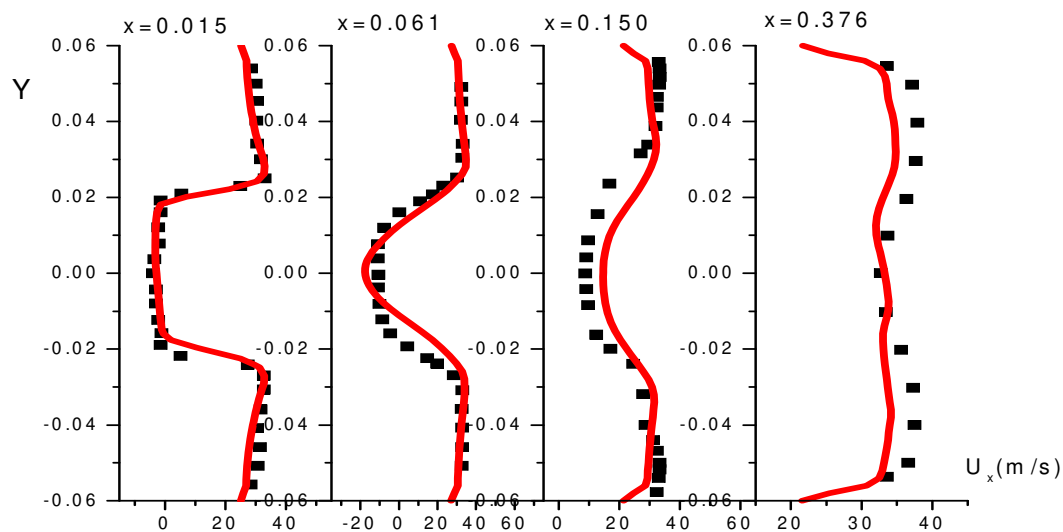
Fig. 12. The averaged x velocity with combustion.
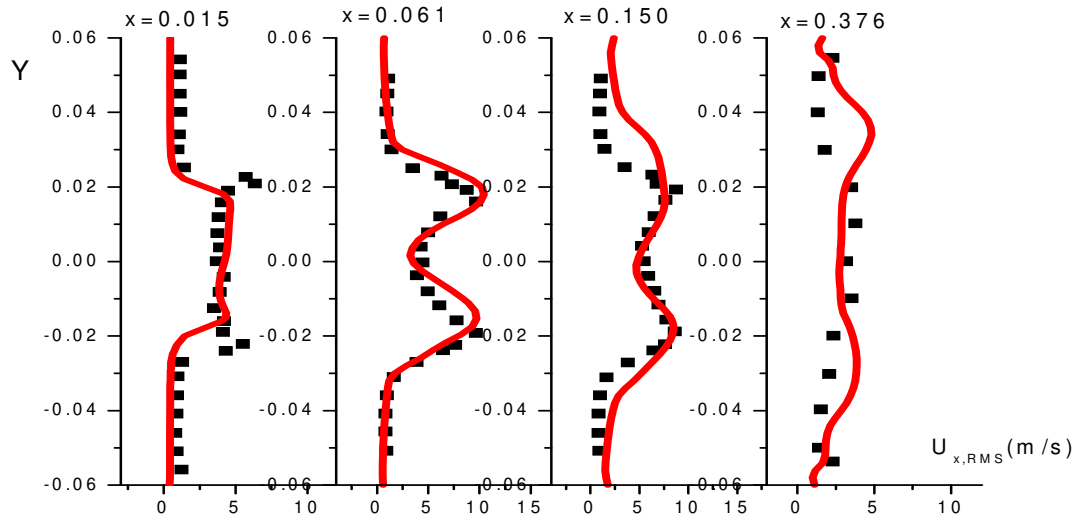


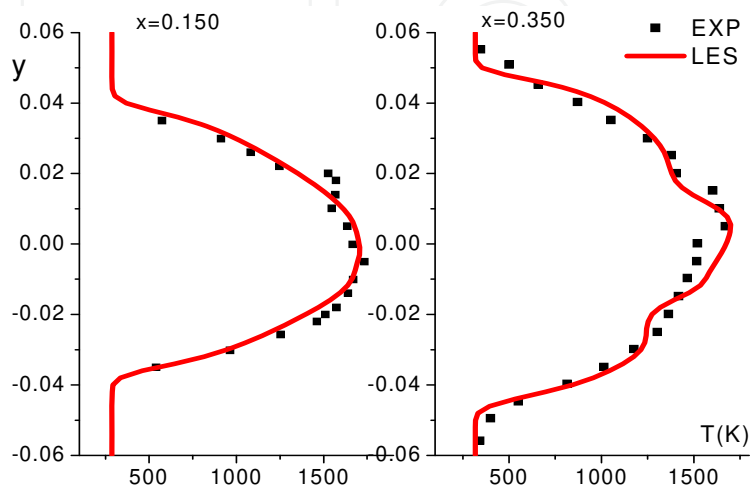Fig. 13. The RMS value of the x velocity with combustion.



Fig. 14. The averaged temperature profiles with combustion.

In figure 15 and 13, the x velocity and its RMS value are compared with the experimental data generally. The predictions are close to the experimental data. Figure 14 is the averaged temperature profiles. The LES predictions are in good agreement with the experimental data. So the LES ASSCM model with the Smagorinsky-Lilly model can properly predict the combustion flow in this premixed case.
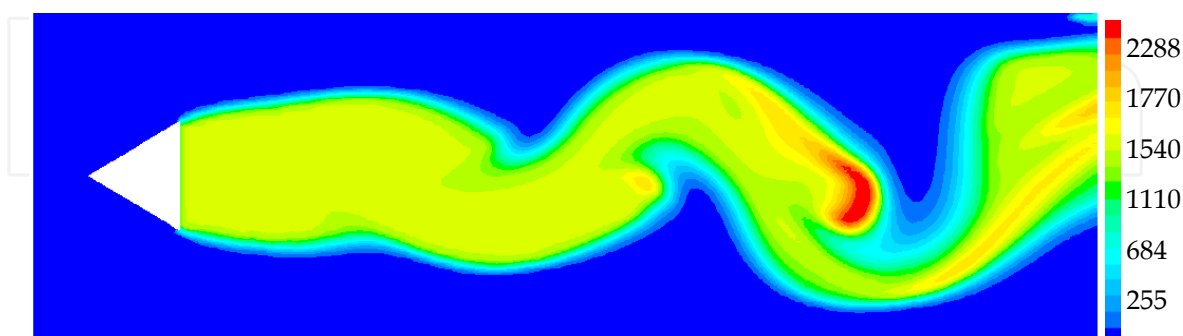


Fig. 15. The instantaneous temperature contour (K).
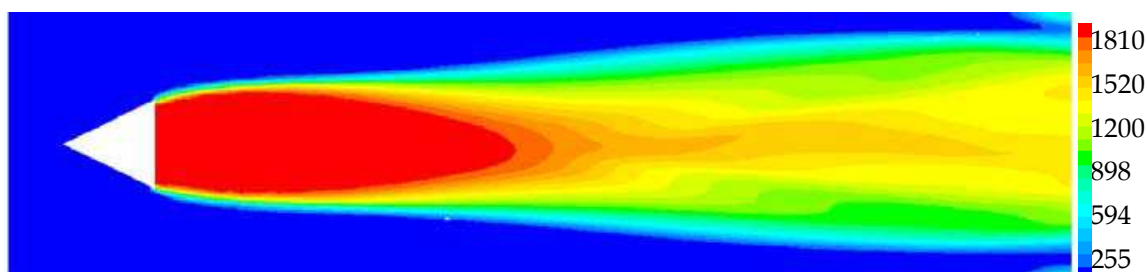


Fig. 16. The averaged temperature contour (K).

The section results are shown in figure 15 and 16: the instantaneous temperature contour and the averaged temperature contour. The bluff body in the combustion chamber works as a flame stabilizer: the premixed flame attached behind the bluff body. The high temperature regions changed a lot in pace with the time steps. The instantaneous high temperature regions are different from the averaged high temperature regions. There are wrinkled flame structures. There are vortex 'source' in the after side of the bluff body. The vortex is generated, stretched and mixed along the combustion chamber.

Because LES method can give much better predictions on turbulent fluctuations, the LES database can be used as a preliminary test source for the RANS combustion model. In RANS USM model, the correlations are solved by transportation equations, such as the transport equation of the correlation of the reaction rate factor K and a species concentration:

$$\frac{\partial}{\partial t}\left(\rho \overline{K'Y'}\right) + \frac{\partial}{\partial x_j}\left(\rho \overline{u_j}\,\overline{K'Y'}\right) = \frac{\partial}{\partial x_j}\left(\frac{\mu_e}{\sigma_g}\frac{\partial \overline{K'Y'}}{\partial x_j}\right) +$$
$$c_{g1}\mu_T \frac{\partial \overline{K}}{\partial x_j}\frac{\partial \overline{Y}}{\partial x_j} - c_{g2}\rho\left(\frac{a}{\tau_A}+\frac{b}{\tau_T}\right)\overline{K'Y'} \tag{10}$$

As for the ASOM model, the expression of the the correlation of the reaction rate factor K and concentration is:

$$\overline{K'Y_1^{'}} = C_{KY_1} \frac{k^3}{\varepsilon^2} \frac{\partial \overline{K}}{\partial x_j} \frac{\partial \overline{Y_1}}{\partial x_j} \tag{11}$$
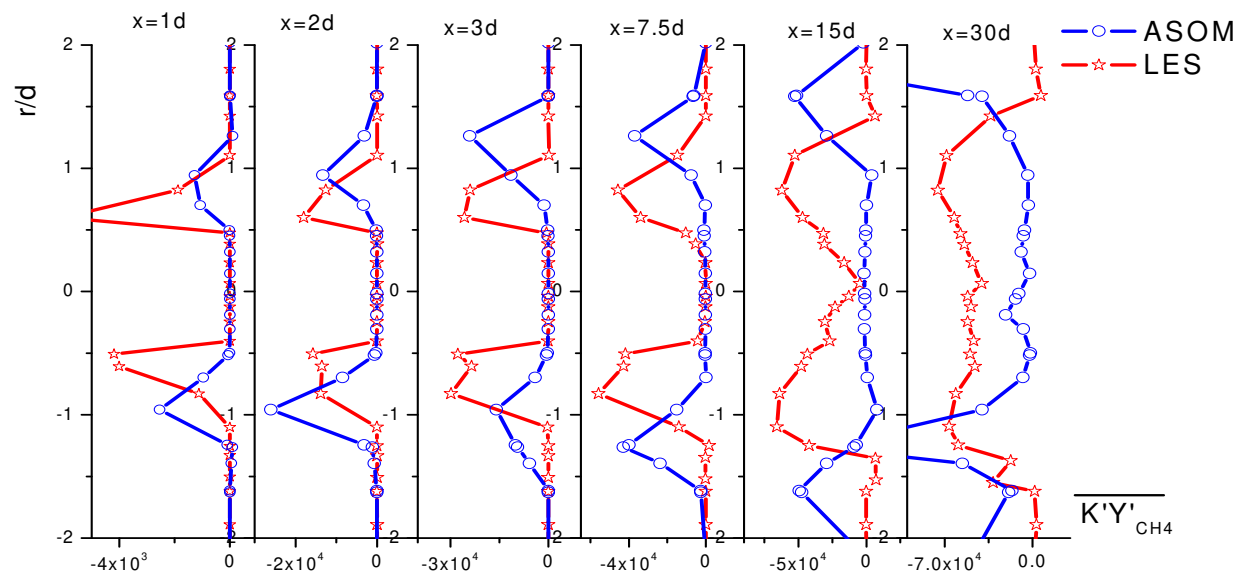


Fig. 17. The correlation comparison between the LES statistic value and ASOM model value.

From the jet flame simulation database here, the RANS ASOM model correlation value is close to the statistic correlation value which is gotten from the LES database, which is shown in figure 17. Generally, the model value is in the same trend with the statistic value and consistent with positive and negative symbols.

The concentration correlation comparison between the model value and the statistic value is shown in figure 18. In most regions, the model values are close to the statistic values. Generally, the model value is of the same magnitude order with the statistic value. The similar statistic calculation is applied in the premixed case too, and the comparison result is shown in figure 19. The model value is close to the statistic value in all the sections.
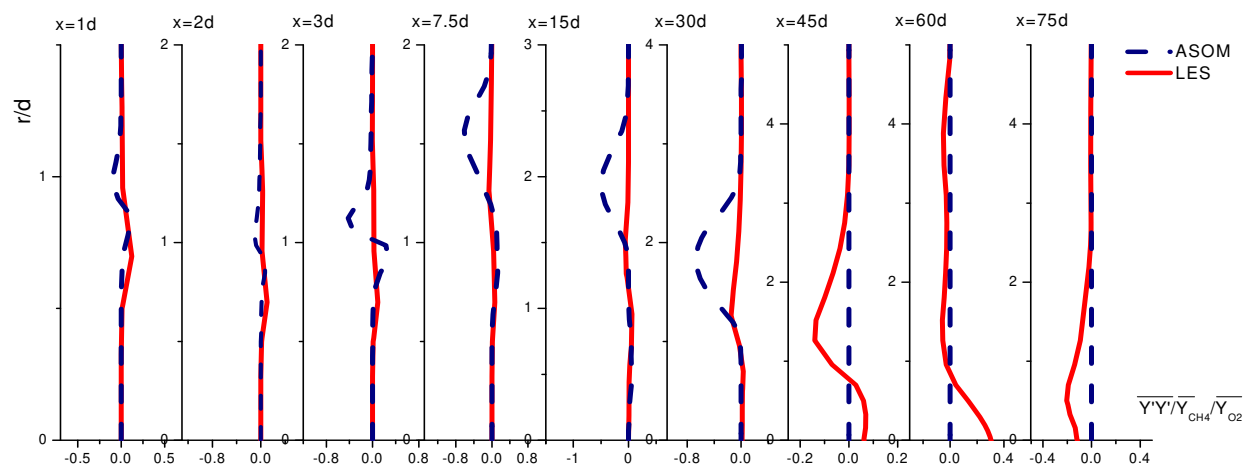


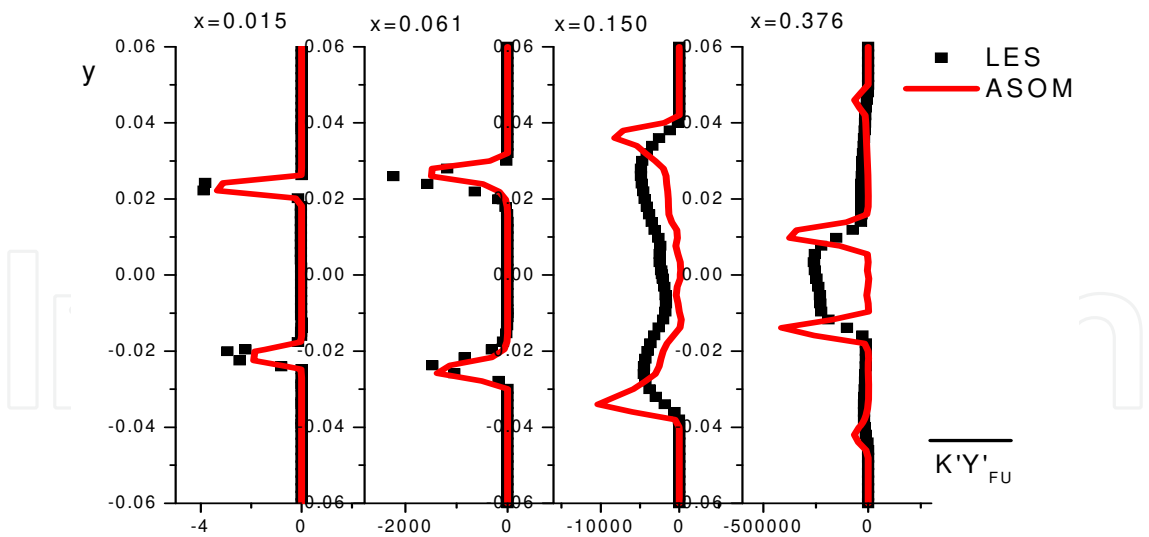Fig. 18. The relative correlation comparison between the LES statistic and ASOM model value.

Fig. 19. The correlation comparison between the LES statistic and ASOM model value.

## 4. Direct numerical simulation for reacting flows

Along with the development of computational technology, direct numerical simulation becomes more and more popular in combustion simulation studies. It is a powerful tool for fundamental study and test sources for RANS and LES models.

In this chapter, a DNS of turbulent reacting channel flows with the consideration of the interaction between the velocity and scalars by buoyancy effect is performed using a spectral method. The instantaneous reaction rate is in Arrhenius form. The computational domain and coordinate system are shown in figure 20. x, y, z are the flow direction, normal direction, and span-wise direction separately. The height of the channel is 2H, the length in the stream-wise is 12.6H and the width in the span-wise direction is 6.28H. The flow is fully developed and the reactants mixed sufficiently.
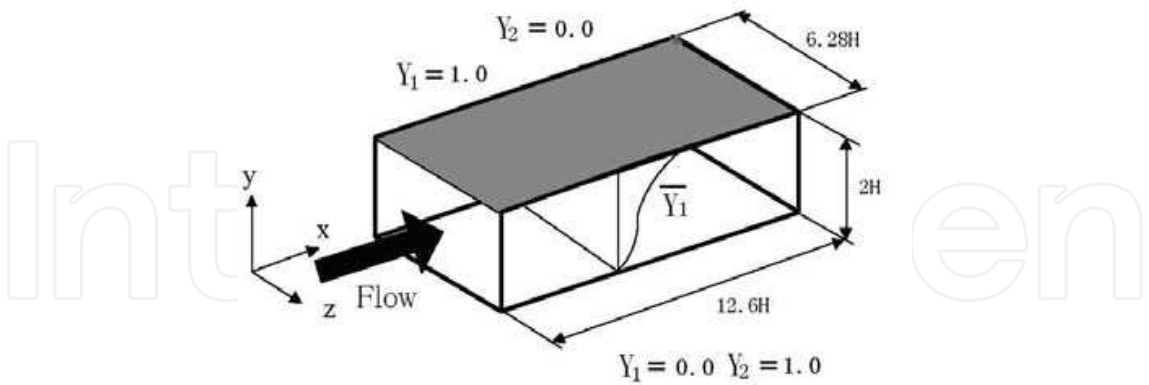


Fig. 20. The computation domain for DNS.

The instantaneous continuity, momentum, species concentration and energy equations of incompressible turbulent reacting flows, with consideration of the buoyancy effect using Boussinesq approximation and taking the Arrhenius expression of one-step kinetics.

$$\frac{\partial u_i}{\partial x_i} = 0$$

(12)

$$\frac{\partial u_i}{\partial t} + u_j \frac{\partial u_i}{\partial x_j} = -\frac{\partial p}{\partial x_i} + \frac{\partial}{\partial x_j}[\nu(\frac{\partial u_i}{\partial x_j} + \frac{\partial u_j}{\partial x_i})] - F_i$$

(13)

$$\frac{\partial}{\partial t}(Y_1) + \frac{\partial}{\partial x_j}(u_j Y_1) = \frac{\partial}{\partial x_j}(D\frac{\partial Y_1}{\partial x_j}) - w_1 / \rho$$

(14)

$$\frac{\partial}{\partial t}(Y_2) + \frac{\partial}{\partial x_j}(u_j Y_2) = \frac{\partial}{\partial x_j}(D\frac{\partial Y_2}{\partial x_j}) - w_2 / \rho$$

(15)

$$\frac{\partial}{\partial t}(T) + \frac{\partial}{\partial x_j}(u_j T) = \frac{\partial}{\partial x_j}(\frac{\lambda}{c_p \rho}\frac{\partial T}{\partial x_j}) + w_1 Q_1 / (c_p \rho)$$

(16)

The $F_i$ term in momentum equation stands for the effect from buoyancy force which caused by the difference of the temperature, also it induces the scalar and velocity interaction. The Reynolds number $Re_m$ defined by the channel half width H and average velocity $U_m$ is 3000. The parameters in DNS cases are given in Table 1.

For all cases, the mass fraction of species 1 (fuel) is given as 1.0 at the top wall and 0.0 at the bottom wall, whereas the mass fraction of species 2 (oxidizer) is given as 0.0 at the top wall and 1.0 at the bottom wall. The wall temperature is given as 900K. Periodic boundary conditions are used in the longitudinal and spanwise directions and solid-wall boundary conditions are used on the top and bottom boundaries.

| Case | B | E/R (K) | Q (kJ/kg) | $F_y$ (m/s²) |
|------|-----|---------|-----------|-------------|
| 1 | 0 | 0 | 0 | 0 |
| 2 | 0.1 | 0 | 0 | 0 |
| 3 | 1.0 | 0 | 0 | 0 |
| 4 | $10^8$ | 15000 | 100 | 0 |
| 5 | $10^8$ | 20000 | 100 | 0 |
| 6 | $10^{10}$ | 20000 | 100 | 0 |
| 7 | $10^8$ | 20000 | 100 | -0.5 |
| 8 | $10^8$ | 15000 | 100 | $F_y$ |
| 9 | $10^8$ | 20000 | 100 | $F_y$ |

Table 1. Parameters for DNS Cases.

For numerical simulations, the Galerkin-Tau spectral expansion method is adopted. The Fourier transform is used in x and z directions and the Chebyshev transform is used in the y direction. Uniform grid distribution is in x and z directions and the Gauss-Lobatto nonuniform grid distribution is used in the y direction. The number of grid nodes in x and z directions is 128, and in the y direction is 129. This results a total of 2.11 million nodes. The time step used is 0.01H/Um. A third-order scheme is used for time marching.

The statistical RMS value of velocities and a correlation were compared with the literature data (Kawamura 2000), which are shown in figure 21 and 22. The predictions from this chapter are labelled by SM DNS, and the predictions from literature are labelled by FD DNS.

In the SM DNS simulation results, $U_\tau=0.063845247$, $Re_\tau=191.54$. The two DNS results are very close to each other.
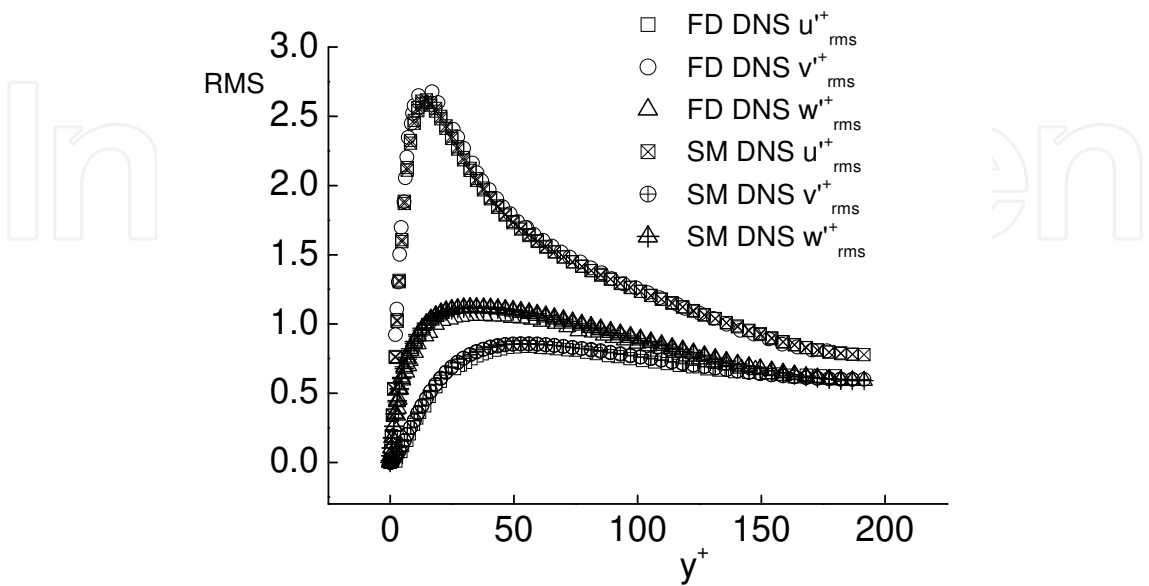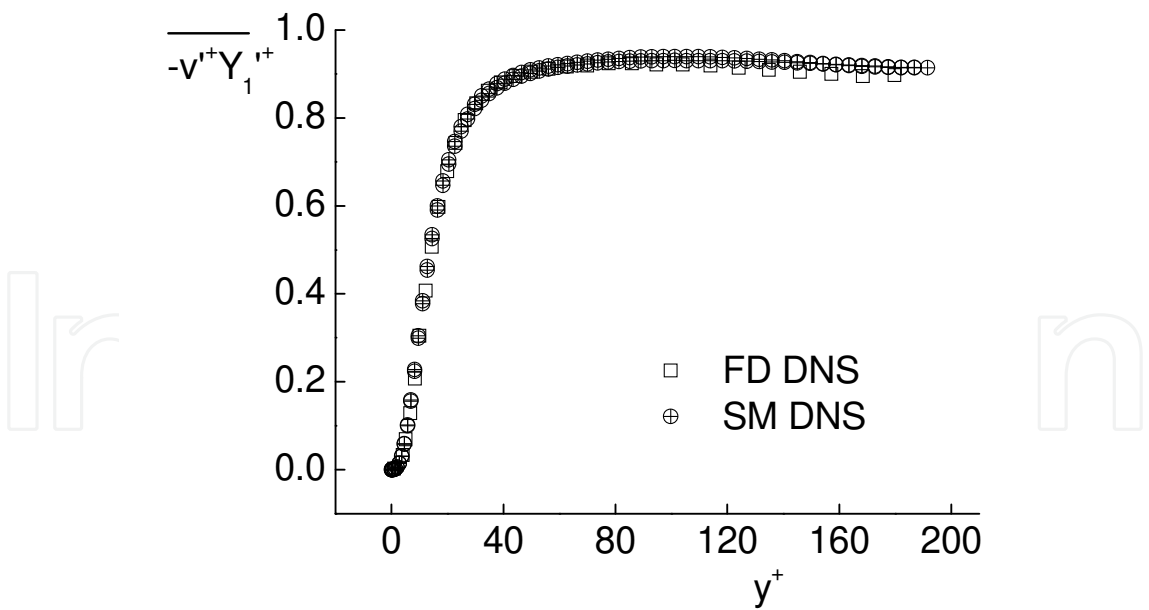
Fig. 21. The RMS value of velocities.

Fig. 22. The averaged value of the correlation of concentration and v velocity

The instantaneous contour of temperature and species are shown in figure 23 and 24. The plenty turbulent structures and near-wall stripe structures can be seen. The statistical averaged reaction factor K profiles is shown in figure 25.
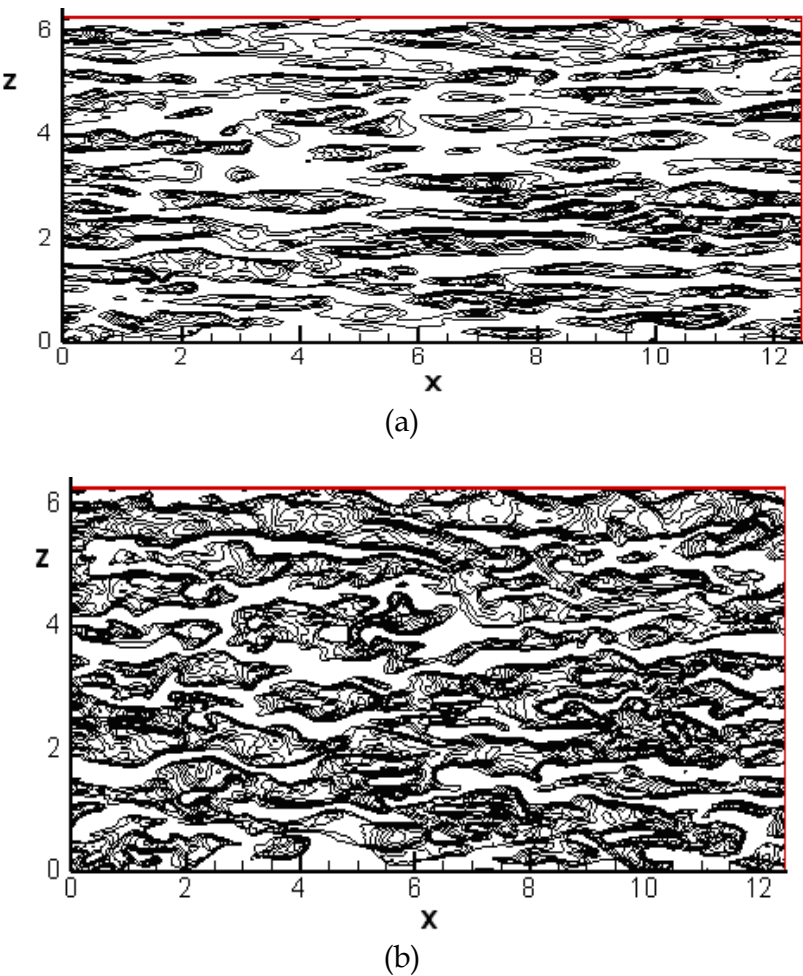
(a)



(b)

Fig. 23. The instantaneous contour of temperature fluctuations in case 5
(a-y$^+$=8.2, b-y$^+$=24.9)
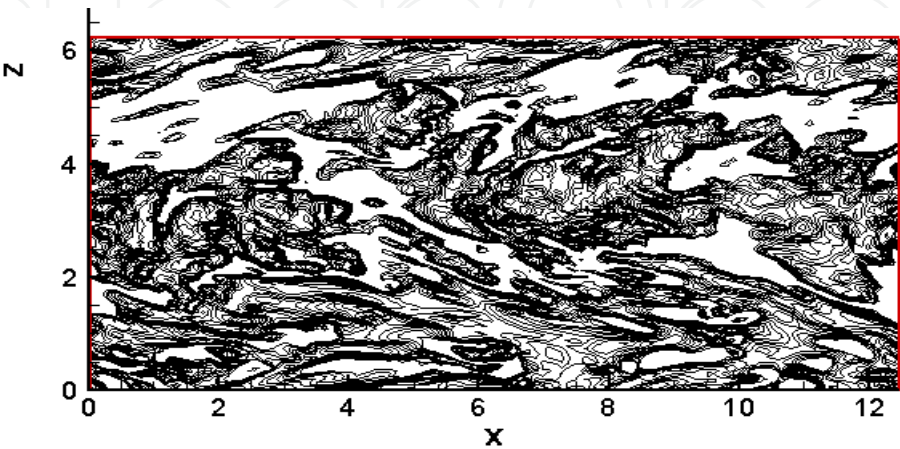


Fig. 24. The instantaneous contour of concentration fluctuation (case 8, y$^+$=8.2)
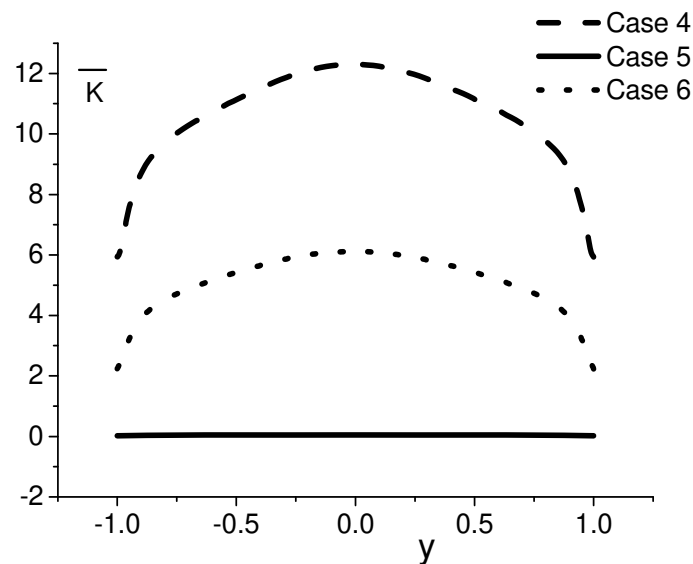
Fig. 25. The averaged reaction factor K profiles.

## 5. Turbulent combustion model study by DNS

The DNS database is used for the scalar fluctuation correlations transportation equations' budget. The exact values are compared with the model values, and then the improvement is given in the turbulent combustion model.

Firstly, a RANS transport equation combustion model is studied. In turbulent combustion model, the correlations are important terms. As for incompressible flow, $c_P$ is constant, $D$ = $\dfrac{\lambda}{\rho c_P}$, and put $w_1 = w_2 = B\rho^2 Y_1 Y_2 \exp(-\dfrac{E}{RT}) = \rho^2 Y_1 Y_2 K$ reaction term into the equations, then the exact transportation equation for $\overline{T'Y_1'}$, $\overline{K'Y_1'}$ and $\overline{Y_1'Y_2'}$ are:

$$\frac{\partial \overline{Y_1'T'}}{\partial t} + \overline{u_j}\frac{\partial \overline{Y_1'T'}}{\partial x_j} = -\overline{T'u_j'}\frac{\partial \overline{Y_1}}{\partial x_j} - \overline{Y_1'u_j'}\frac{\partial \overline{T}}{\partial x_j} - \frac{\partial \overline{u_j'Y_1'T'}}{\partial x_j} +$$
$$D\frac{\partial}{\partial x_j}(\frac{\partial \overline{Y_1'T'}}{\partial x_j}) - 2D\overline{\frac{\partial T'}{\partial x_j}\frac{\partial Y_1'}{\partial x_j}} + \frac{\rho Q_1}{c_P}\overline{Y_1'Y_1Y_2K} - \rho\overline{T'Y_1Y_2K}$$

(17)

$$\frac{\partial \overline{K'Y_1'}}{\partial t} + \overline{u_j}\frac{\partial \overline{K'Y_1'}}{\partial x_j} = -\overline{u_j'K'}\frac{\partial \overline{Y_1}}{\partial x_j} - \overline{u_j'Y_1'}\frac{\partial \overline{K}}{\partial x_j} - \frac{\partial \overline{u_j'K'Y_1'}}{\partial x_j} +$$
$$D\frac{\partial}{\partial x_j}(\frac{\partial \overline{K'Y_1'}}{\partial x_j}) - 2D\overline{\frac{\partial Y_1'}{\partial x_j}\frac{\partial K'}{\partial x_j}} - \frac{\lambda}{\rho c_P}\frac{E}{R}\overline{\frac{Y_1'}{T^2}\frac{\partial K}{\partial x_j}\frac{\partial T}{\partial x_j}} -$$
$$\frac{2\lambda}{\rho c_P}\overline{\frac{Y_1'}{T}\frac{\partial K}{\partial x_j}\frac{\partial T}{\partial x_j}} - \rho\overline{K'Y_1Y_2K} + \frac{E\rho Q_1}{Rc_P}\overline{\frac{Y_1'KY_1Y_2K}{T^2}}$$

(18)

$$\frac{\partial \overline{Y_1'Y_2'}}{\partial t} + \overline{u_j}\frac{\partial \overline{Y_1'Y_2'}}{\partial x_j} = -\overline{u_j'Y_2'}\frac{\partial \overline{Y_1}}{\partial x_j} - \overline{u_j'Y_1'}\frac{\partial \overline{Y_2}}{\partial x_j} - \frac{\partial \overline{u_j'Y_1'Y_2'}}{\partial x_j} +$$

$$D\frac{\partial}{\partial x_j}(\frac{\partial \overline{Y_1'Y_2'}}{\partial x_j}) - 2D\overline{\frac{\partial Y_1'}{\partial x_j}\frac{\partial Y_2'}{\partial x_j}} - \rho\overline{Y_1'Y_1Y_2K} - \rho\overline{Y_2'Y_1Y_2K}$$

(19)

The statistical correlation values are shown in figure 26 to 29. The temperature fluctuation is very important in reaction correlations. Then the budgets are studied and shown in figure 30 to 32. In these results, $\overline{K'Y_1'}$ value changes greatly and $\overline{T'Y_1'}$ are more important than $\overline{Y_1'Y_2'}$ according to the average value.
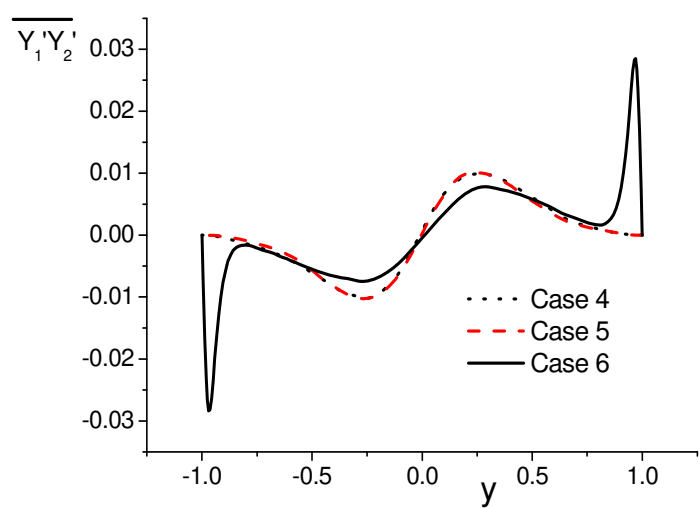


Fig. 26. The profiles of the $\overline{Y_1'Y_2'}$ .
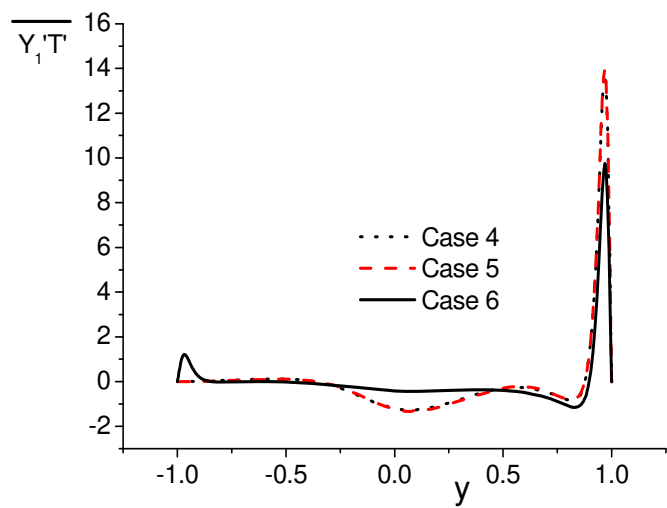


Fig. 27. The profiles of the $\overline{T'Y_1'}$ .
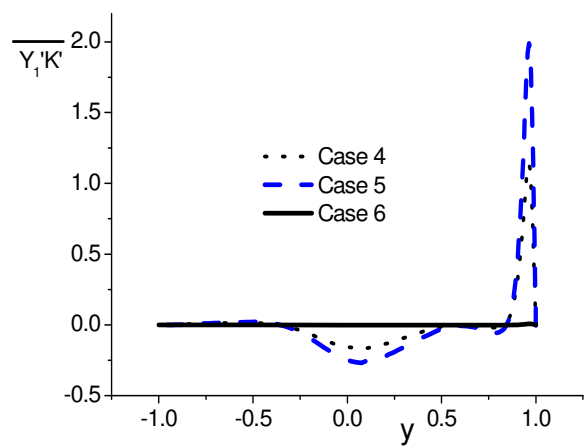
Fig. 28. The profiles of the $\overline{K'Y_1'}$.
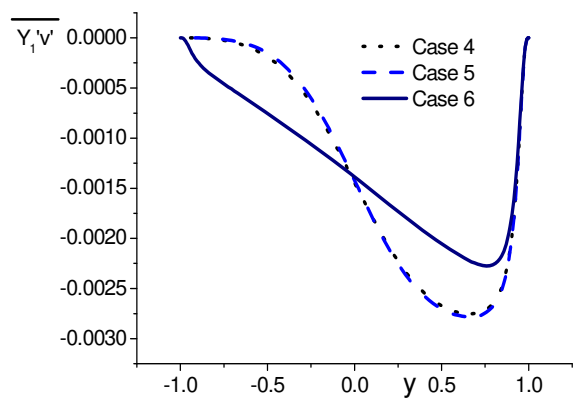


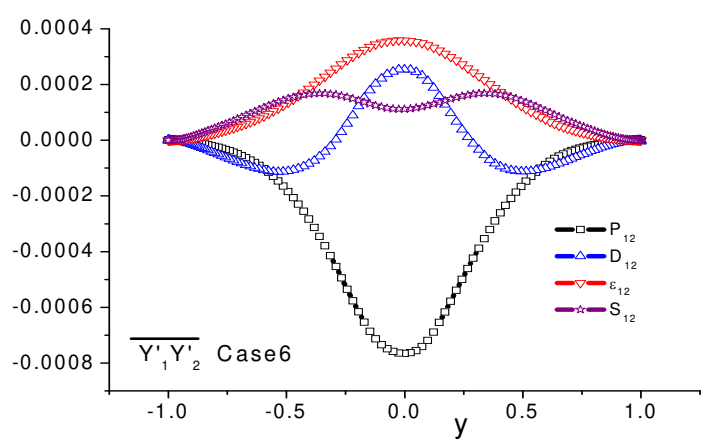Fig. 29. The profiles of the $\overline{v'Y_1'}$.



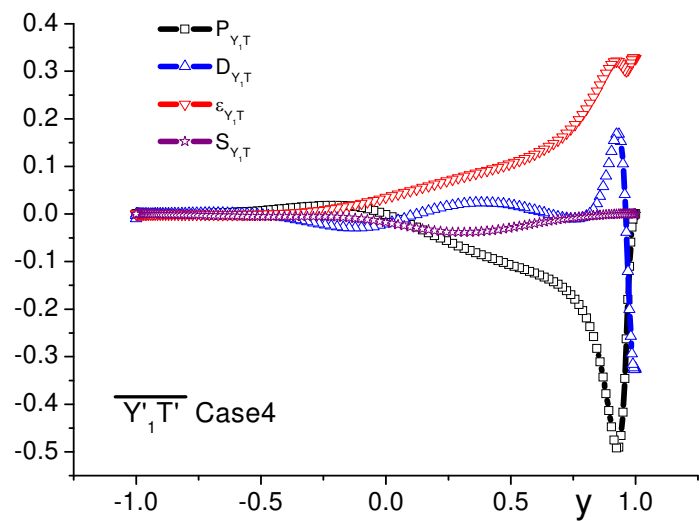Fig. 30. The budget of the $\overline{Y_1'Y_2'}$ equation.

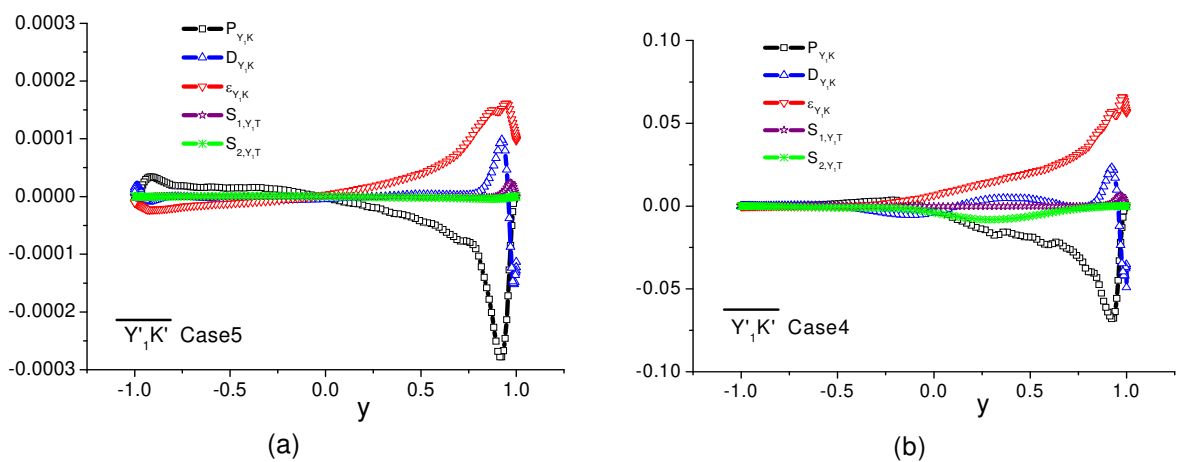Fig. 31. The budget of the $\overline{T'Y_1'}$ equation.



Fig. 32. The budget of the $\overline{K'Y_1'}$ equation.

From the magnitude and distribution, the chemistry affects a lot in correlations and their budget. In RANS model, the correlation transportation equations need to be closed with the production term, turbulent diffusion term and the dissipation term. As for the production term, the isotropic turbulent model is applied with $\sigma_Y$ = 0.7. It is assumed that the dissipation of the correlation is direct proportion to itself. And gradient model is used in the diffusion term.

$$\frac{\partial \overline{K'Y_1'}}{\partial t} + \overline{u_j} \frac{\partial \overline{K'Y_1'}}{\partial x_j} = \frac{C_1 \mu_t}{\rho \sigma_{KY}} \frac{\partial \overline{Y_1}}{\partial x_j} \frac{\partial \overline{K}}{\partial x_j} + \frac{\mu_e}{\sigma_{KY}} \frac{\partial}{\partial x_j} (\frac{\partial \overline{K'Y_1'}}{\partial x_j})$$
$$-C_2 \frac{\varepsilon}{k} \overline{K'Y_1'} - C_3 [B\rho(\overline{Y_1} + \beta\overline{Y_2})\exp(-\frac{E}{R\overline{T}})]\overline{K'Y_1'}$$

(20)

$$\frac{\partial \overline{Y_1' Y_2'}}{\partial t} + \overline{u_j} \frac{\partial \overline{Y_1' Y_2'}}{\partial x_j} = \frac{C_1 \mu_t}{\rho \sigma_{YY}} \frac{\partial \overline{Y_1}}{\partial x_j} \frac{\partial \overline{Y_2}}{\partial x_j} + \frac{\mu_e}{\sigma_{YY}} \frac{\partial}{\partial x_j} (\frac{\partial \overline{Y_1' Y_2'}}{\partial x_j})$$

$$-C_2 \frac{\varepsilon}{k} \overline{Y_1' Y_2'} - C_3 [B\rho(\overline{Y_1} + \beta \overline{Y_2}) \exp(-\frac{E}{R\overline{T}})] \overline{Y_1' Y_2'}$$

(21)

In which, $C_1 = 11.5$, $\sigma_{KY} = \sigma_{YY} = 0.7$, $C_2 = 0.005$, $C_3 = 0.012$, $\beta = 1.0$.

The comparison of the DNS exact values and the RANS model values are shown in figure 33 and 34. Generally, the model values of the production term (a), diffusion term (b) and the total dissipation term (c) are close to the exact values from DNS database. The difference between the exact values and the model values is rooted from the model assumption.
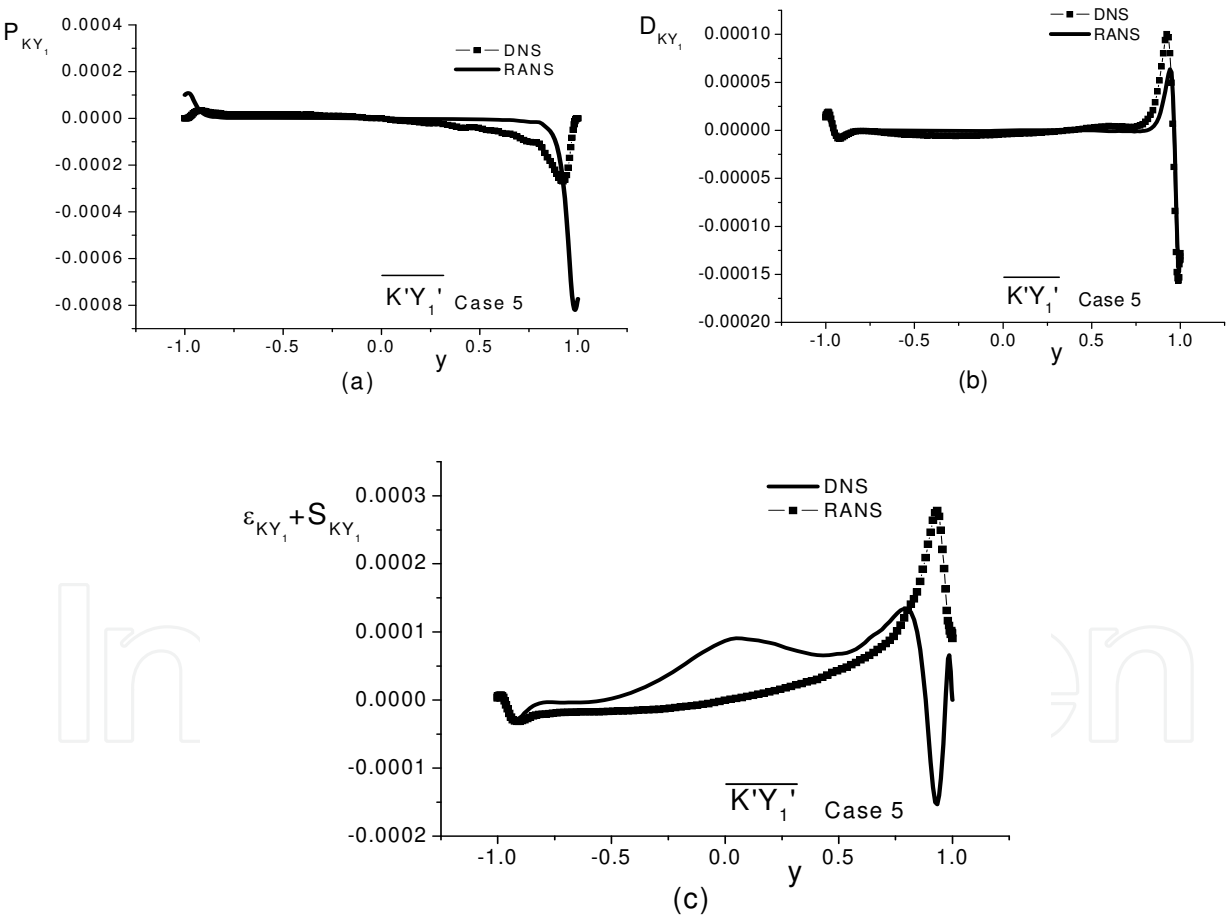


Fig. 33. The DNS statistical value and RANS model value of terms in $\overline{K' Y_1'}$ correlation equation in case 5.
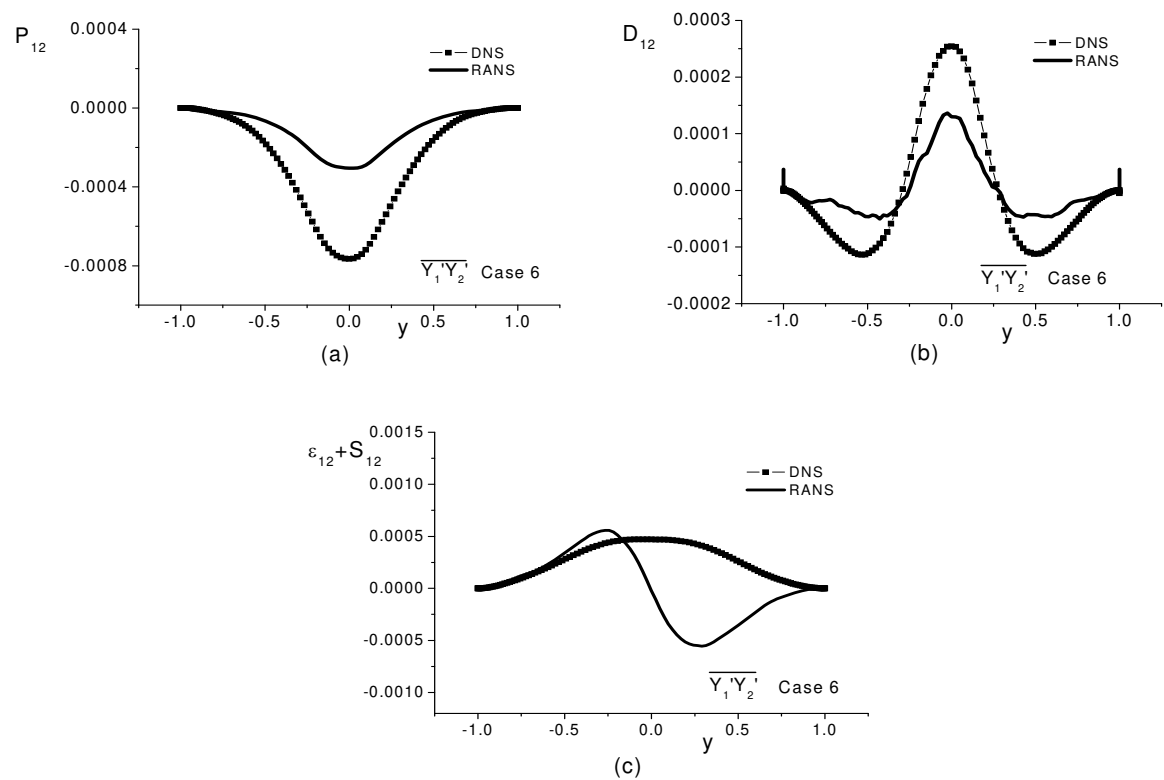
Fig. 34. The DNS statistical value and RANS model value of terms in $\overline{Y_1'Y_2'}$ correlation equation in case 6.

The algebraic second order moment (ASOM) RANS turbulent combustion model is quite simple but have been applied in jet flame successfully. The model expression is:

$$\overline{Y_1'Y_2'} = C_{YY} \frac{k^3}{\varepsilon^2} \frac{\partial \overline{Y_1}}{\partial x_j} \frac{\partial \overline{Y_2}}{\partial x_j} \tag{22}$$
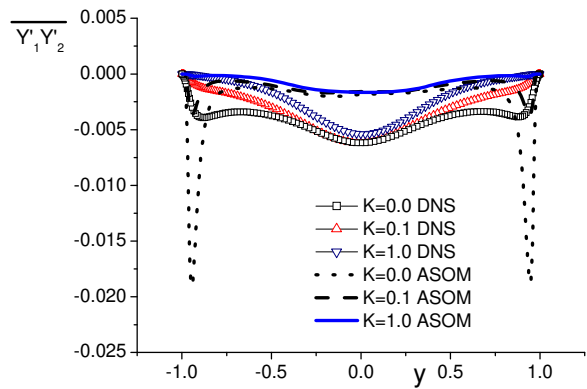
$$\overline{K'Y_1'} = C_{KY_1} \frac{k^3}{\varepsilon^2} \frac{\partial \overline{K}}{\partial x_j} \frac{\partial \overline{Y_1}}{\partial x_j} \tag{23}$$



Fig. 35. The DNS statistical value and RANS model value of correlation $\overline{Y_1'Y_2'}$

The comparison between DNS exact values and the algebraic model values are shown in figure 35 and 36. The model values are in same trend with the exact values while in some regions, the model values are rather of distortion. The overestimated value in the near wall regions and the underestimations in the main flow regions resulted from the gradient simplification. The model constant in ASOM model is 0.005. These results show the reasonableness of ASOM model.
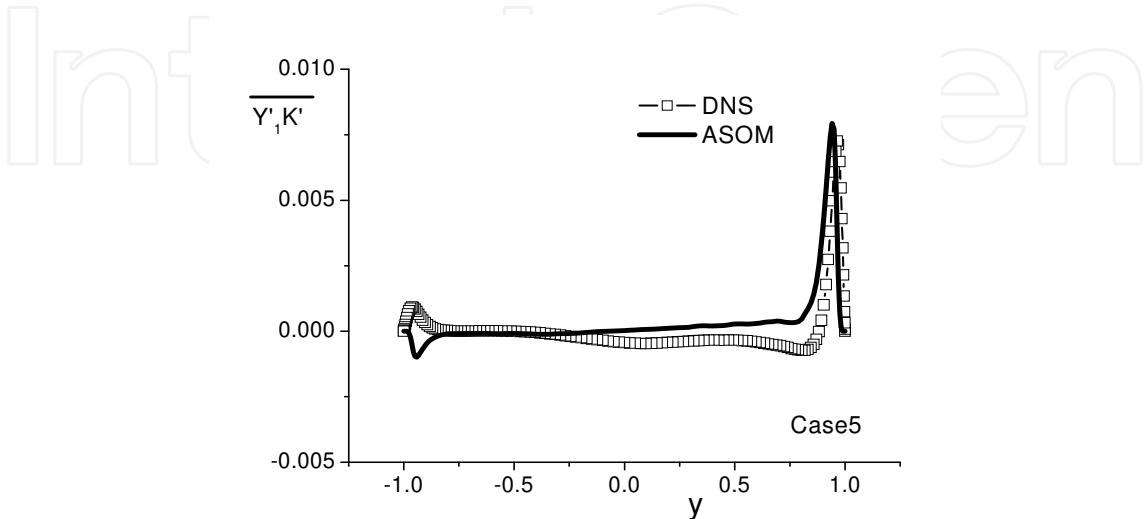


Fig. 36. The DNS statistical value and RANS model value of correlation $\overline{K'Y_1'}$.

As for the ASSCM SGS model in LES, the small scale reaction is calculated by:

$$\widetilde{Y_1 Y_2 K} - \tilde{Y}_1 \tilde{Y}_2 \tilde{K} = \tilde{K}(\widetilde{Y_{OX} Y_{Fu}} - \tilde{Y}_{OX} \tilde{Y}_{Fu}) + \tilde{Y}_{OX}(\widetilde{K Y_{Fu}} - \tilde{K}\tilde{Y}_{Fu}) + \tilde{Y}_{Fu}(\widetilde{K Y_{OX}} - \tilde{K}\tilde{Y}_{OX}) \qquad (24)$$

The three quasi-correlation parts in the right hand side, shortened as $R_{Y_1 Y_2}$, $R_{Y_1 K}$ and $R_{Y_1 T}$, are

$$R_{\Phi\Psi} = \widetilde{\Phi\Psi} - \tilde{\Phi}\tilde{\Psi} = C_{\Phi,\psi} L_S^2 \frac{\partial \tilde{\Phi}}{\partial x_j} \frac{\partial \tilde{\Psi}}{\partial x_j} \qquad (25)$$

Initially, the turbulent model is Smagorinsky-Lilly SGS model with $L_S = C_S \Delta$. While this model get bigger dissipation in flow regions especially in the near wall region, then a damping correction is used [zhang 2005]:

$$L_S = C_S \Delta [1 - \exp(-y^+ / A^+)], \ C_S = 0.2, \ A^+ = 26 \qquad (26)$$

In the spectral method, each variable in flow can be expended as Fourier function, in this chapter, the DNS wave number is 128, then assumed that the cut-off wave number in LES is 64, thus the DNS results can be divided into two parts: the low-pass value represents the resolvable value in LES and the rest high order value represents the sub-grid scale value. Using the filtering function, the statistic value of SGS correlation $R_{Y_1 K}$ and $R_{Y_1 T}$ from DNS database and SGS model value are shown in figure 37 to 42. $R_{Y_1 T}$ and $R_{Y_1 K}$ have same trend, and they have similar distribution in all domain.
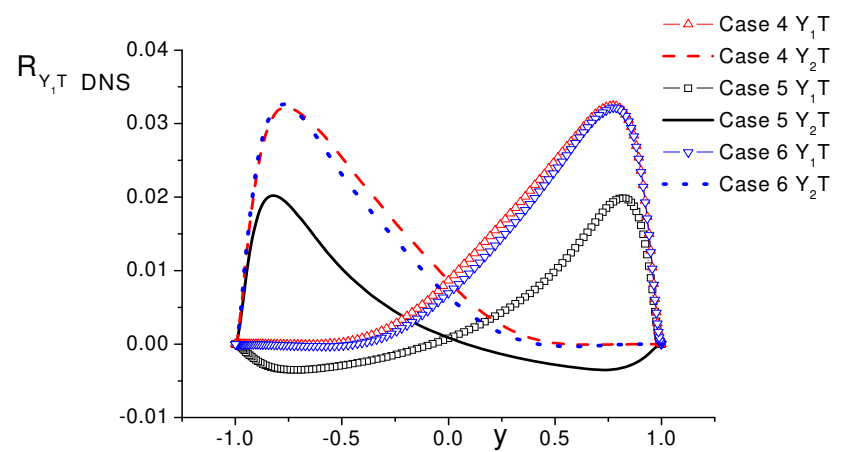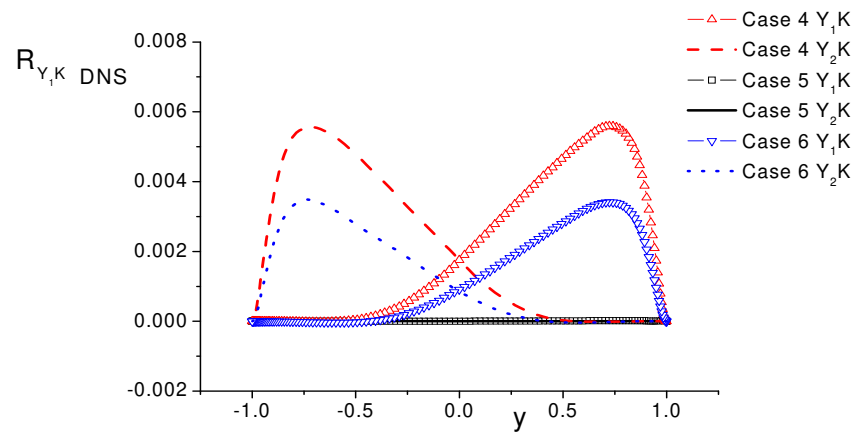
Fig. 37. The DNS value of SGS $R_{Y_1 T}$ .



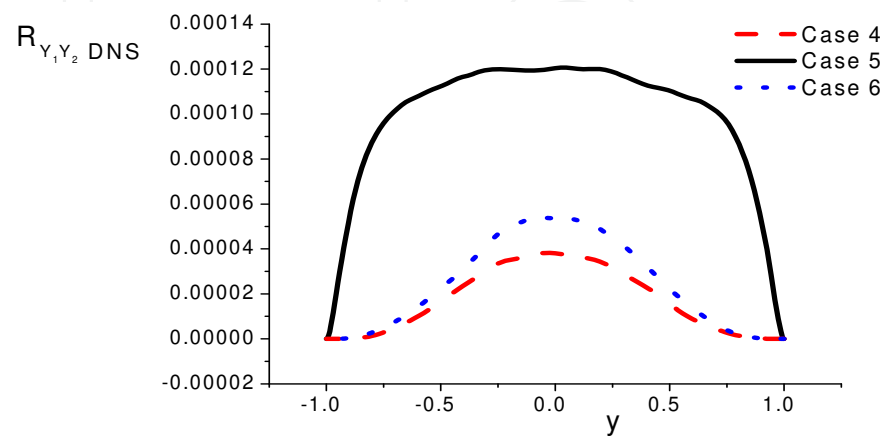Fig. 38. The DNS value of SGS $R_{Y_1 K}$ .
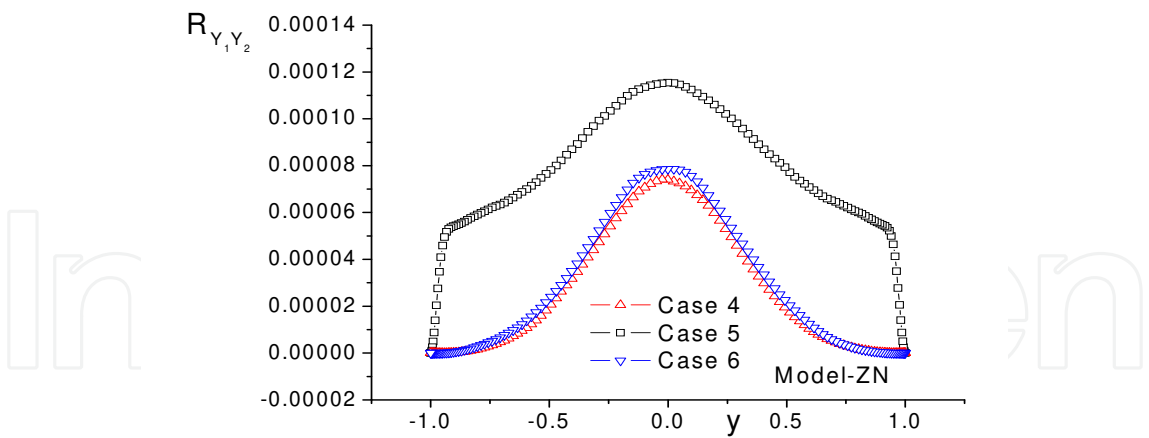


Fig. 39. The DNS value of SGS $R_{Y_1 Y_2}$ .

Fig. 40. The DNS value of SGS $R_{Y_1Y_2}$ with wall correction.

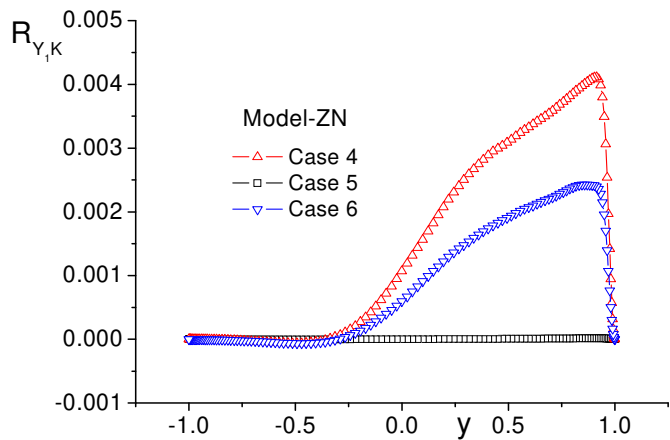

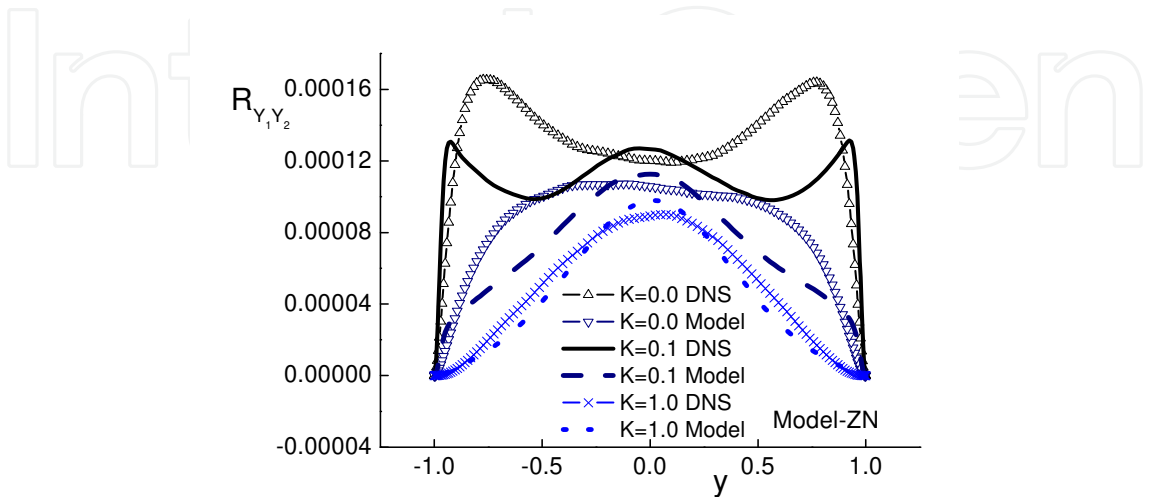Fig. 41. The DNS value of SGS $R_{Y_1K}$ with wall correction.



Fig. 42. The DNS value of SGS $R_{Y_1Y_2}$ with wall correction

In ASSCM turbulent SGS combustion model, the model factor is constant, while the exact value for model factor is shown in figure 43. It can be treat as a constant in most regions, but changes a lot in the near wall regions and varies according to different cases.



(a)                                                                                       (b)
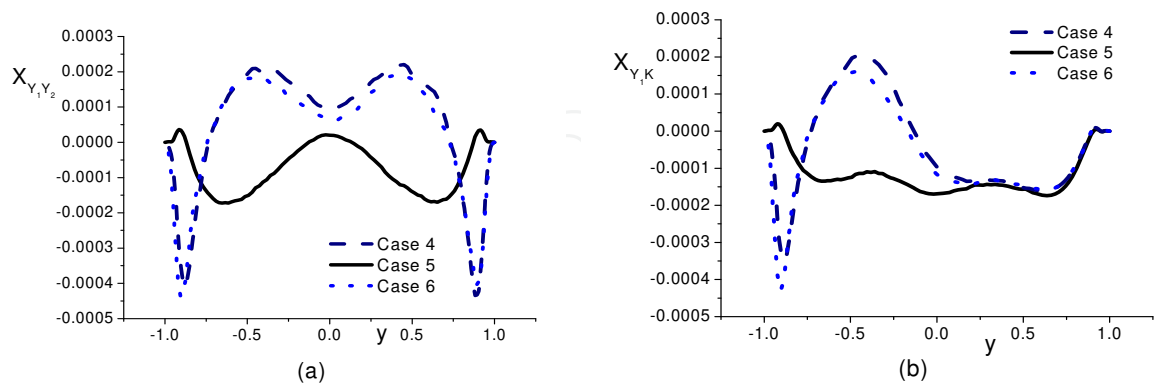
Fig. 43. The SGS model factor from DNS statistic.

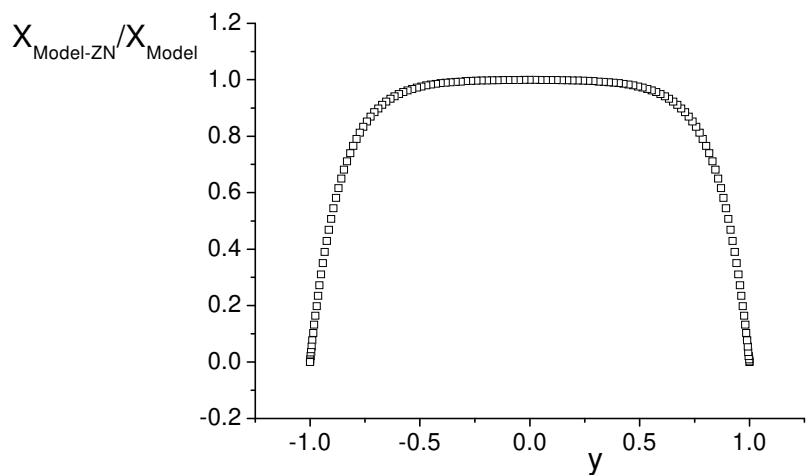While the model factor value with the near wall damping modification is shown in figure 44.



Fig. 44. The modified SGS model factor ($X_{Model-ZN}$) divided by constant model value ($X_{Model}$)

According to the figures above, it is clearly that the modified model ($X_{Model-ZN}$) is better than the constant value model ($X_{Model}$) in the near wall regions because its value is closer to the exact DNS statistic value, so the damping model can give more reasonable prediction results.

The SGS scalar flux model is using gradient model with damping modification:

$$g_{u_j Y_1} = C_{u_j Y_1} \frac{\gamma_T}{\sigma} \frac{\partial \tilde{Y}_1}{\partial x_j} \tag{27}$$

Sum up the main points in this part, briefly, there are typical strip structures in the velocity and scalar field. The chemical reaction enhanced the turbulence especially in high shear regions. In the transportation equations of correlations, the production term and the dissipation term are more important. Comparison with the exact value from DNS, the RANS second order moment turbulent combustion model and the RANS algebraic second order

moment turbulent model can give reasonable predictions in most regions. The damping modification model can give better prediction results than the constant value model because it is closer to the exact model factor value.
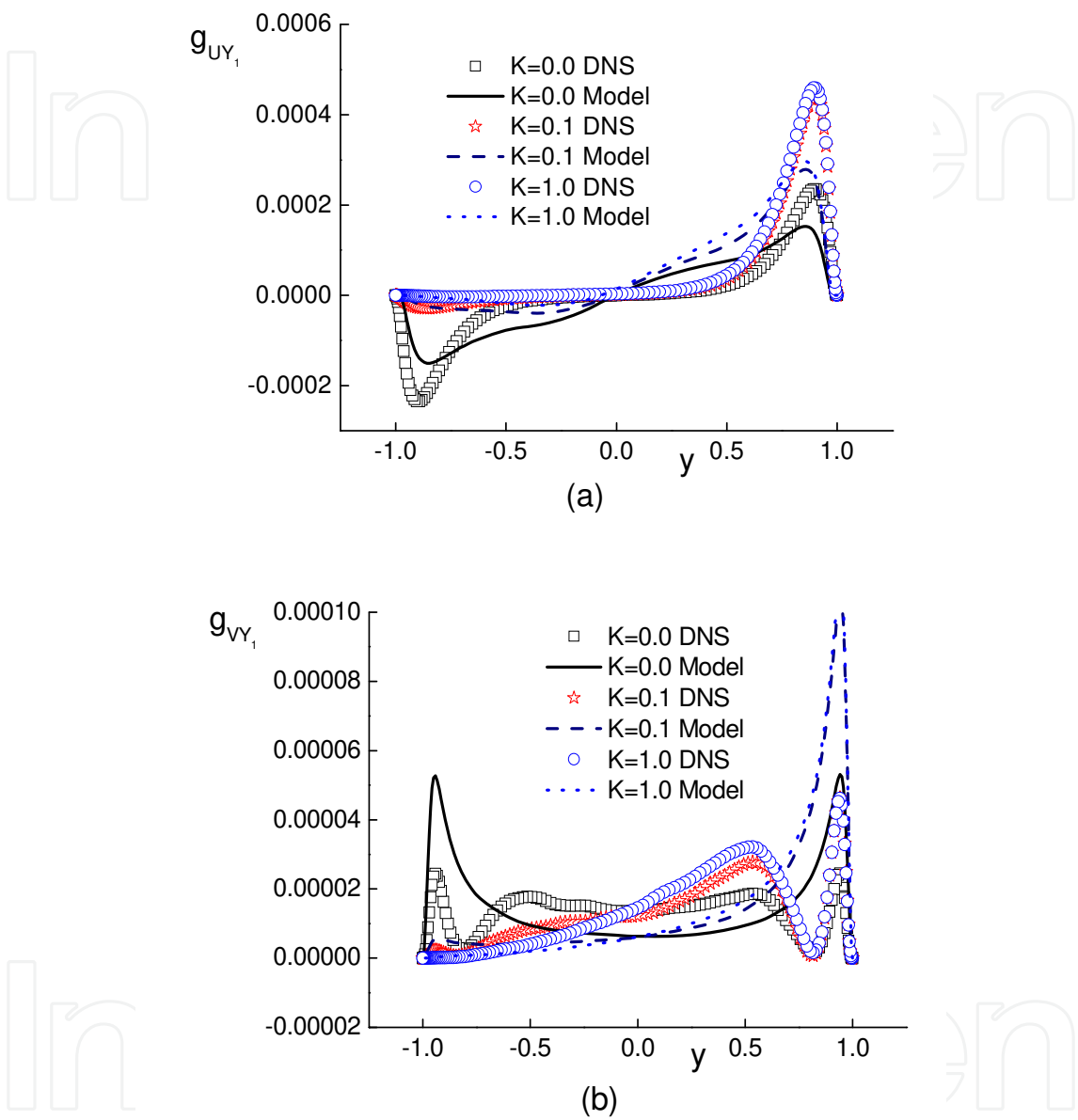


Fig. 45. The SGS flux model tested with damping model.

## 6. Conclusion

The LES and DNS methods are more and more important recently. There are many SGS turbulent combustion models for LES. The algebraic sub-grid scale turbulent combustion is quite simple in expression, while it is successfully applied in partly diffusion jet flame and premixed after bluff body flame. The predicted temperature, species, velocity and RMS values are all close to the experimental data in the most regions.

A spectral method DNS is carried in a channel reaction flow. The results are used for turbulent model research. It is shown that the ASSCM SGS model value is close to the exact value mainly, so ASSOM model is reasonable again.

The ASOM RANS turbulent combustion model is tested by LES and DNS results. Though this model is simple, its value has same trend with the exact value and quite close to the exact value sometimes. It can give quick and roughly prediction for average parameters but not RMS value.

The correlations in turbulent combustion model are studied in DNS, the temperature fluctuation is very important. The RANS equations were modelled. The near wall damping modification can improve the prediction ability of SGS model.

## 7. References

Colucci P J, Jaberi F A, Givi P. Filtered density function for large eddy simulation of turbulent reacting flows. Physics of Fluids, 1998, 10(2):499~515

DesJardin P E, Frankel S H. Two-dimensional large eddy simulation of soot formation in the near-field of strongly radiating nonpremixed acetylene-air turbulent jet flame. Combustion and Flame, 1999, 119:121~123

Gao F, Obrien E E. A large-eddy simulation scheme for turbulent reacting flows. Phys Fluids A, 1993, 5(6):1282~1284

Giacomazzi E, Battaglia V, Bruno C. The coupling of turbulence and chemistry in a premixed bluff-body flame as studied by LES. Combustion and Flame, 2004, 138:320~335

James S, Jaberi F A. Large scale simulations of two-demensional nonpremixed methane jet flames. Combustion and Flame, 2000, 123:465~487

Jones W P. Large eddy simulation of turbulent combustion processes. Computer Physics Communications, 2002, 147:533~537

Kawamura H, Abe H, Shingai K. DNS of turbulence and heat transport in a channel flow with different Reynolds and Prandtl numbers and boundary conditions. In: Nagano Y, Hanjalic K, Tsuji, eds. 3rd Int. Symp. on Turbulence, Heat and Mass Transfer. Tokyo, 2000. 15~32

Renfro M W, Chaturvedy A, King G B. Comparison of OH time-series measurements and large-eddy simulations in hydrogen jet flames. Combustion and Flame, 2004, 139:142~151

Westbrook C K, Dryer F L. Simplified Reaction Mechanisms for the Oxidation of Hydrocarbon Fuels in Flames, Combust. Sci. Tech. 1981, 27(1-2): 31-43

Xu C, Toonder J M J, Nieuwstadt F T M, et al. Origin of high kurtosis levels in the viscous sublayer. Direct numerical simulation and experiments. Physics of Fluids, 1996, 8(7):1938~1944

Yaga M, Endo H, Yamamoto T, et al. Modeling of eddy characteristic time in LES for calculating turbulent diffusion flame. International Journal of Heat and Mass Transfer, 2002, 45:2343~2349

Zhang Z S, Cui G X, Xu C X, Theory and modelling of turbulence, Beijing, Qsinghua University Press, 2005

**Computational Simulations and Applications**

Edited by Dr. Jianping Zhu

ISBN 978-953-307-430-6

Hard cover, 560 pages

**Publisher** InTech

**Published online** 26, October, 2011

**Published in print edition** October, 2011

The purpose of this book is to introduce researchers and graduate students to a broad range of applications of computational simulations, with a particular emphasis on those involving computational fluid dynamics (CFD) simulations. The book is divided into three parts: Part I covers some basic research topics and development in numerical algorithms for CFD simulations, including Reynolds stress transport modeling, central difference schemes for convection-diffusion equations, and flow simulations involving simple geometries such as a flat plate or a vertical channel. Part II covers a variety of important applications in which CFD simulations play a crucial role, including combustion process and automobile engine design, fluid heat exchange, airborne contaminant dispersion over buildings and atmospheric flow around a re-entry capsule, gas-solid two phase flow in long pipes, free surface flow around a ship hull, and hydrodynamic analysis of electrochemical cells. Part III covers applications of non-CFD based computational simulations, including atmospheric optical communications, climate system simulations, porous media flow, combustion, solidification, and sound field simulations for optimal acoustic effects.

# INTECH

open science | open minds